Università degli Studi di Salerno
Dipartimento di Matematica

Doctoral Dissertation

OLD AND NEW PROBLEMS IN CONTINUUM STRUCTURAL MATERIALS

Massimo Pecoraro

Dottorato di Ricerca in Matematica
PhD Program in Mathematics
XII ciclo

Coordinator:
Patrizia Longobardi

Advisor:
Ettore Laserra

Co-advisors:
Gaetano Caricato and Mauro Fabrizio

Contents

List of Figures

Introduction

This PhD thesis, which deals with old and new issues for structural materials of a continuous, is divided into four chapters. The first two chapters, are related to Old Problems studied in previous years of PhD and further explored during its course as the classic arguments of continuum mechanics. In particular, the first chapter deals with that some microscopic structures of the skeleton in the higher vertebrates, precisely the osteones, approximately, have the shape of transversely isotropic small hollow cylinders. Their biomechanical behaviour has been carefully studied and a connection has been mentioned between this behaviour and the Volterra's distortions. So G. Caricato proposed an extension of that theory in the case of a transversally isotropic homogeneous elastic hollow cylinder. In this first chapter it has been reconsidered and expanded the findings to obtain explicit formulas for the equilibrium equations, for the boundary conditions, for the vector field of displacements and for tensor fields of strain and stress, while the second chapter deals with that In the context of Volterra's partially results, analyzes the forces induced by the sixth elementary distortion on the right circular, homogenous, hollow, isotropic cylinder with a different point of view. More precisely, exploiting Saint Venant's theory and generalizing some previous results, I have underlined that, apart from a limited zone in the immediate vicinity of bases, the distribution of forces, considered as a specific load, can be replaced with one statically equivalent. This can be done without consequences on the effective distributions of stress and strain, and therefore, without the necessity to define the effective punctual distribution of this load acting on the bases of the cylinder. Because of the homogeneity and isotropy of the material and of the geometric and loading symmetry of the body, I have approached the specific load as linear, constructed an auxiliary bar which has as longitudinal section the axial section of the cylinder and followed the basic considerations of Saint Venant's theory. I have found the specific load connected to the sixth distortion is equivalent (in Saint Venant's theory) to a right combined compressive and bending stress and to a right combined tensile and bending stress. This chapter is organized as follows: in section 2 the general theory of Volterra's distortions is briefly recalled. In section 3 the specific load is analyzed by Saint Venant's theory. In section 4 numerical results and their comparison with Volterra's predictions are discussed. The last two chapters are related to problems on new theories relating to continuous bodies: New Problems studied during years of PhD as the new arguments of continuum mechanics. In particular, the tird chapter deals with on the theory of the passage of a material from the paramagnetic behavior to that of ferromagnetic and vice-versa. Ferromagnetism is a typical phenomenon occurring in materials such as iron, cobalt, nickel and many alloys containing these elements. The ferromagnetic phase appears when a small external magnetic field yields

a large magnetization inside the material, due to the alignment of the spin magnetic moments. Moreover, we observe a residual magnetization; namely, the spin magnetic moments stay aligned even if the external magnetic field vanishes. It is well-known that ferromagnetic materials are characterized by a critical temperature θ_c, called the Curie temperature. For temperatures greater than θ_c, the material shows a paramagnetic behaviour. When the temperature crosses θ_c, the material undergoes a second order transition and displays ferromagnetic behaviour. In ferromagnetic materials I observe an easy magnetization, motivated by the property of atom patterns to displays a magnetic moment. In this work I propose a model for describing the para-ferromagnetic phase transition and for predicting the classical hysteresis loops bellow the critical temperature θ_c. The large magnetic field is due to the alignment patterns of their constituent atoms, which act as elementary electromagnets. By an order parameter or phase field we mean a macroscopic variable describing the internal physical state of the material, given by some macroscopic (chemical and physical) properties. In the para-ferromagnetic transition we observe a different behavior of the order parameter, which characterizes the nature of the transition. According to the modern classification due to Landau, phase transitions can be separated into two classes: first and second order transitions. In first order transitions, as long as θ does not cross θ_c, the phase field is a constant function in both the phases. This does not happen in second order transitions, in which the order parameter is constant in one of two phases only. In other papers, on all paramagnetic and ferromagnetic phases, the order parameter is not a constant, but a function of the magnetic field. In this work, in agreement with the definition of a second order phase transition, we propose a model such that in the paramagnetic phase the order parameter is a new variable, independent from magnetic field. Finally, within this range, we obtain the peculiar hysteresis loops characteristic of a hard magnet; while the fourth chapter deals with that in a shape memory alloys, it observe a structural transformation between austenite and martensite phase, called martensite phase transition. These materials are capable to recover permanent strain when are heated over a given temperature. At high temperature the crystal lattice of the material is in a high symmetric phase, called austenite (A). At low temperature we observe the martensite phase (M), represented by a smaller symmetry. This transformation is crystallographically reversible. Moreover, the variations of the stress and temperature have a large influence on these transformations. So to generate force and thermal changes through a phase transition. For the study of these materials, we follow the approach presented by the notion of order parameter or phase field φ and the use of the Ginzburg-Landau (G-L) theory of phase transitions, together to the classical equations of thermomechanics. In this work I have considered two different potentials in G-L equation, which provide more convenient numerical simulations for the stress-strain diagrams. Moreover, these two new potentials are able to well describe some SMAs, as the Single Crystal AuZn, for which the character of the transformation lies at a borderline between a continuous and discontinuous phase transition. So that, this new free energy describes an intermediate behavior within a first and second order phase transition. In other words, the differential system differs from other classic SMA models because now the transformation is described by a continuous transition between austenite and martensite phase. Following, the G-L equation is obtained as a balance law on the internal structure of the material, and then as a new field equation to which to associate a new internal power to be considered in the First Law of

Thermodynamics. In the model, the G-L, the motion and heat equations are related by a differential constitutive equation on the strain, stress and order parameter. Finally, I study some numerical simulations for 1-D problem, for which now the order parameter and the free energy take a different representation compare to 3-D model. Nevertheless, this 1-D problem describes the same intermediate behavior between a continuous and discontinuous transitions. Our study begin with the explicit field equations for 3-D model, describing shape memory alloys. Here, the several variants of martensite are described by the product $\varepsilon\varphi$, where ε is the strain, fixed by crystallographic structure and $\varphi \in [0, 1]$. The model is in agreement with the typical damping capacity and fatigue life of a SMAs. Then, I study the compatibility of the model with the Thermodynamic Laws. So, I obtain the potentials: internal energy, free energy and entropy. In the last section, I present a one-dimensional model, for which now the order parameter $\varphi \in [-1, 1]$. Thus, this model is not a special case of the 3-D model. The work finishes with some numerical simulations, that provide the classical stress-strain diagrams of SMAs.

Chapter 1

The theory of distortions in continuum mechanics

In this chapter it will be considered the Volterra's theory of elastic dislocations in the case of a transversally isotropic homogeneous hollow cylinder. It will be obtained explicit equations of vector field of displacements, of tensor fields of strain and stress, and of forces upon the boundary [37].

1.1 Introduction

" *The researches of V. Volterra in the field of elastic dislocations* [1] *are considered an admirable and perfect work of Mathematical–Physics...* [30]" (see e.g. [52, 42, 3]). Recently it has been shown that some microscopic structures of the skeleton in the higher vertebrates, precisely the osteones, approximately, have the shape of transversely isotropic small hollow cylinders. Their biomechanical behaviour has been carefully studied [2] and a connection has been mentioned between this behaviour and the Volterra's distortions. So G. Caricato proposed an extension of that theory in the case of a transversally isotropic homogeneous elastic hollow cylinder [17]. [2]

In this work we will reconsider and expand the findings [17]; we will obtain explicit formulas for the equilibrium equations, for the boundary conditions, for the vector field of displacements and for tensor fields of strain and stress [3].

Thus we are presenting the following:

- That the hypothesis in [17] of the parallelism of the two vectors $\mathbf{h}$ and $\mathbf{k}$, characteristic of the displacement (1.3), plays no role in our research.
- From the analysis of the equilibrium equations we show that the coefficient l_3, present in the displacement (1.3) and arbitrarily retained in the notes [17], assumes instead the expression (1.21), so the displacement (1.3) depends only on the parameters a_1 and l_4. The strain (1.37) and the stress (1.25) are calculated from the following form (1.23) of the displacement: they only depend on the parameters a_1 and l_4. From examining the boundary conditions we can then deduce the coefficient l_3 vanishes and as a consequence the parameter a_1 assumes the explicit form (1.34).
- The final displacement (1.35), together with the strain (1.37) and stress (1.38) tensors, become exclusively dependent on the arbitrary parameter l_4. The only components of the strain and stress tensors depending on the parameter l_4 are ϵ_{13}, ϵ_{23} and σ_{13}, σ_{23} respectively.
- The vector field displacement becomes dependent on the rapport N/A of only two of the five elastic constants which characterize the transversally isotropic case.
- Finally we have found under which conditions Volterra's formulas (1.2) for the isotropic case can be attained again.

It remains to be calculated, in a following work, a generic auxiliary displacement $\mathbf{u}'$, to obtain the complete explicit form of Volterra's dislocations in the case under examination (see [17], par.2.1, note 5).

[1] Volterra calls the deformations which his theory refers to *"distortions"*, Love prefers to call them *"dislocations"*, (see [42], Art. 156, note pag. 221)

[2] In his note on distorsions Volterra studies the equilibrium of multi–connected elastic homogeneous bodies, particularly hollow cylinders, limiting his study only to isotropic bodies.

[3] We have utilized the Computer Algebra System *Mathematica*, which allows not only to verify the calculations rapidly, but also automatically generates the LaTeX sources of formulas.

1.2 Volterra's dislocations in the case of an isotropic homogeneous hollow cylinder

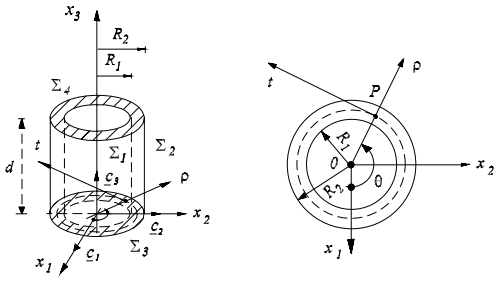

Figure 1.1: The hollow cylinder in the natural state and one of its cross sections

Briefly let's refer to Volterra's dislocations theory, limiting it to the case of cylinder $\mathcal{C}$, circular, hollow (therefore doubly connected), homogeneous, elastic and isotropic, which is found, at a certain assigned temperature τ, in a natural state $\mathcal{C}_\tau^*$, and assumed as a reference configuration [4]. So we introduce into an ordinary space a cartesian rectangular reference $O\,x_1x_2x_3$ of respective versors $\{\mathbf{c_1}, \mathbf{c_2}, \mathbf{c_3}\}$. We choose the axis $O\,x_3$ coinciding with the symmetry axis of the cylinder and the coordinate plane $O\,x_1x_2$ placed over the base ${\alpha^*}_1$; $d = (x_3)_{{\alpha^*}_2} > 0$ is the height of the base ${\alpha^*}_2$. Finally Σ^* is the lateral surface of $\mathcal{C}^*$, made from the two cylindrical coaxial surfaces ${\Sigma^*}_1$ (internal surface of radius r) and ${\Sigma^*}_2$ (external surface of radius R). P^* is the generic point of $\mathcal{C}_\tau^*$, $\theta = \arctan\frac{x_2}{x_1}$ is the anomaly of P^* and $\rho = \sqrt{{x_1}^2 + {x_2}^2}$ is the distance of P^* from the axis of the cylinder. Since the cylinder $\mathcal{C}$ is doubly connected, many–valued displacements $\mathbf{u}$ are possible (see e.g. [42], art. 156 p. 221).

Volterra used Weingarten's note [54] as a starting point, where it is shown that an elastic body occupying a dominion, not simply connected, can find itself in a state of tension also in the absence of external forces. Volterra developed a general theory, with some improvements from Cesaro (see e.g. [52] and [42] Art. 156 pag. 221). Volterra began with the observation that Weingarten's considerations could not be validated in the case of simply–connected bodies in the range of regular deformations. With this in mind he constructed his well–known Volterra's formulas, which obtain the displacements of the points of an elastic body, once assigned the linearized tensor of deformation. Then he examined the field of displacements

[4] The theory of dislocations initially has a very general character, but subsequently is substantially focused to obtain explicit results in the study of equilibrium of hollow homogeneous and *isotropic* cylinders.

whose cartesian components are [5]

$$\begin{cases} u_1 = \dfrac{1}{2\pi}(\, l + qx_3 - rx_2)\,\theta + (\, ax_1 + bx_2 + cx_3 + e)\,\log\rho^2 \\ u_2 = \dfrac{1}{2\pi}(\, m + rx_1 - px_3)\,\theta + (\, a'x_1 + b'x_2 + c'x_3 + e')\,\log\rho^2 \\ u_3 = \dfrac{1}{2\pi}(\, n + px_2 - qx_1)\,\theta + (\, a''x_1 + b''x_2 + c''x_3 + e'')\,\log\rho^2 \end{cases} \tag{1.1}$$

where the two triplets (l, m, n) and (p, q, r) are the respective cartesian components of the two assigned constant vectors $\mathbf{h} \equiv (l, m, n)$ and $\mathbf{k} \equiv (p, q, r)$. He determined the twelve constants $a, b, c, e;\ a', b', c', e';\ a'', b'', c'', e''$ so that the three functions (1.1) would verify the equilibrium equations (see e.g. [52] pag. 428); so he obtained the formulas

$$\begin{cases} u_1 = \dfrac{1}{2\pi}\left\{(l + qx_3 - rx_2)\,\theta + \dfrac{1}{2}\left(-m + px_3 + \dfrac{r\mu}{\lambda + 2\mu}x_1\right)\log\rho^2\right\} \\ u_2 = \dfrac{1}{2\pi}\left\{(m + rx_1 - px_3)\,\theta + \dfrac{1}{2}\left(l + qx_3 + \dfrac{r\mu}{\lambda + 2\mu}x_2\right)\log\rho^2\right\} \\ u_3 = \dfrac{1}{2\pi}\left\{(n + px_2 - qx_1)\,\theta - \dfrac{1}{2}(px_1 + qx_2)\,\log\rho^2\right\} \quad , \end{cases} \tag{1.2}$$

where λ and μ are the two Lamé constants (see e.g. [30]).

He observed the displacement (1.2) generates a distribution of forces not identically vanishing on the surface of the cylinder. So he calculated a supplementary field of displacements $\mathbf{u}'(P^*)$ single–valued, which would satisfy the indefinite equations of elastic equilibrium in the absence of forces of mass and would generate the same distribution of surface forces on the boundary of the cylinder. The field of displacements

$$\mathbf{u}''(P^*) = \mathbf{u}(P^*) - \mathbf{u}'(P^*)$$

satisfies the indefinite equations of equilibrium equally, but does not generate any distribution of forces on the boundary of the cylinder and is many–valued like $\mathbf{u}(P^*)$. [6]

The many–valued field of displacements $\mathbf{u}''(P^*)$ can be physically interpreted through the following operations (see e.g. [42] pag. 224):

1. By making a transversal cut on an axial semi–plane, we make the hollow homogeneous cylinder $\mathcal{C}_\tau$ simply–connected and it assumes a natural state $\mathcal{C}_\tau^*$. We'll call the two faces of the cut γ_1^* and γ_2^*.

2. We'll impose a translatory displacement $\mathbf{h} \equiv (l, m, n)$ and a rotatory displacement $\mathbf{k} \equiv (p, q, r)$ to one of the two faces, e.g. γ_1^*, with respect to the other. The two characteristic vectors $\mathbf{h}$ and $\mathbf{k}$ together will be parallel to the semi–plane π. In this way making the face γ_1^* penetrate into γ_2^* or distance itself from γ_2^* according to the vector $\mathbf{k}$ will levogyrous or dextrogyrous accordingly.

[5] Conforming to [17, 30] the p, q, r are opposing signs with respect to Volterra's original work (see e.g. [52] pag. 427).

[6] So we obtain the real Volterra's dislocation, which consists of two parts: the many–valued main displacement $\mathbf{u}(P^*)$ and the single–valued supplementary displacement $-\mathbf{u}'(P^*)$.

3. If $\mathbf{k}$ is levogyrous we'll remove a thin slice of matter, a thickness proportional to the distance from the axis of the cylinder. If instead $\mathbf{k}$ is dextrogyrous we'll add a thin slice of matter, the same material as the cylinder, between the two faces of the cut, a thickness still proportional to the distance from the axis of the cylinder. In this way we create a state of deformation in the cylinder and therefore of stress.

4. Finally we'll remake the cylinder doubly connected by soldering the two faces of the cut. In this way the cylinder assumes a helicoidal configuration absent of superficial forces and results in a state of regular internal stress.

Collectively, Volterra called the described operations a *dislocation* whose characteristics are $l, m, n,\ p, q, r$ (see e.g. [52]).

1.3 Volterra's dislocations in the case of a transversally isotropic homogeneous hollow cylinder

Now let's consider a *transversally isotropic* [7] elastic homogeneous hollow cylinder and let's suppose it is found in a natural state $\mathcal{C}^*_\tau$ [8] at temperature τ.

In analogy to Volterra's procedure, conforming to [17], let's consider a displacement of the following type:

$$\mathbf{u}(P^*) = \frac{1}{2\pi}(\mathbf{h} + \mathbf{k} \wedge OP^*)\,\theta + \\ + [(\mathbf{a} \cdot OP^* + a_4)\,\mathbf{c}_1 + (\mathbf{b} \cdot OP^* + b_4)\,\mathbf{c}_2 + (\mathbf{l} \cdot OP^* + l_4)\,\mathbf{c}_3]\,\log\rho^2 \tag{1.3}$$

where we can assign the two vectors $\mathbf{h}$ and $\mathbf{k}$, characteristic of the dislocation, while we have to determine yet the vectors $\mathbf{a}$, $\mathbf{b}$, $\mathbf{l}$ and the constants a_4, b_4, l_4.

If we project (1.3) onto the axis we obtain

$$\begin{cases} u_1 = \dfrac{1}{2\pi}(h_1 + k_2x_3 - k_3x_2)\,\theta + (a_1x_1 + a_2x_2 + a_3x_3 + a_4)\,\log\rho^2 \\ u_2 = \dfrac{1}{2\pi}(h_2 + k_3x_1 - k_1x_3)\,\theta + (b_1x_1 + b_2x_2 + b_3x_3 + b_4)\,\log\rho^2 \\ u_3 = \dfrac{1}{2\pi}(h_3 + k_1x_2 - k_2x_1)\,\theta + (l_1x_1 + l_2x_2 + l_3x_3 + l_4)\,\log\rho^2 \end{cases} \tag{1.4}$$

[7] Since it conserves its mechanical characteristics along any direction perpendicular to the axis of symmetry.
[8] Therefore absent of external mass and/or superficial forces.

The displacement gradient $\nabla\mathbf{u} \equiv \left\| \frac{\partial u_h}{\partial x_k} \right\|$ relative to the displacement (1.3),(1.4) is

$$
\begin{cases}
\frac{\partial u_1}{\partial x_1} = & \frac{1}{2\pi\rho^2}(4\pi a_4 x_1 - h_1 x_2 + 4\pi a_1 x_1^2 + 4\pi a_2 x_1 x_2 + 4\pi a_3 x_1 x_3 + k_3 {x_2}^2 - k_2 x_2 x_3) + \\
& + a_1 \log\rho^2 \\
\frac{\partial u_1}{\partial x_2} = & \frac{1}{2\pi\rho^2}(h_1 x_1 + 4\pi a_4 x_2 - (k_3 - 4\pi a_1) x_1 x_2 + 4\pi a_2 x_2^2 + k_2 x_1 x_3 + 4\pi a_3 x_2 x_3) + \\
& - \frac{k_3}{2\pi}\theta + a_2 \log\rho^2 \\
\frac{\partial u_1}{\partial x_3} = & \frac{k_2}{2\pi}\theta + a_3 \log\rho^2 \\
\frac{\partial u_2}{\partial x_1} = & \frac{1}{2\pi\rho^2}(4\pi b_4 x_1 - h_2 x_2 + 4\pi b_1 x_1^2 - (k_3 - 4\pi b_2) x_1 x_2 + 4\pi b_3 x_1 x_3 + k_1 x_2 x_3) + \\
& + \frac{k_3}{2\pi}\theta + b_1 \log\rho^2 \\
\frac{\partial u_2}{\partial x_2} = & \frac{1}{2\pi\rho^2}(h_2 x_1 + 4\pi b_4 x_2 + k_3 {x_1}^2 + 4\pi b_1 x_1 x_2 + 4\pi b_2 x_2^2 - k_1 x_1 x_3 + 4\pi b_3 x_2 x_3) + \\
& + b_2 \log\rho^2 \\
\frac{\partial u_2}{\partial x_3} = & - \frac{k_1}{2\pi}\theta + b_3 \log\rho^2 \\
\frac{\partial u_3}{\partial x_1} = & \frac{1}{2\pi\rho^2}(4\pi l_4 x_1 - h_3 x_2 + k_2 x_1 x_2 - k_1 x_2^2 + 4\pi l_1 x_1^2 + 4\pi l_2 x_1 x_2 + 4\pi l_3 x_1 x_3) + \\
& - \frac{k_2}{2\pi}\theta + l_1 \log\rho^2 \\
\frac{\partial u_3}{\partial x_2} = & \frac{1}{2\pi\rho^2}(h_3 x_1 + 4\pi l_4 x_2 - k_2 x_1^2 + (k_1 + 4\pi l_1) x_1 x_2 + 4\pi l_2 x_2^2 + 4\pi l_3 x_3) + \\
& + \frac{k_1}{2\pi}\theta + l_2 \log\rho^2 \\
\frac{\partial u_3}{\partial x_3} = & l_3 \log\rho^2
\end{cases}
\tag{1.5}
$$

and the components of the strain tensor

$$
\boldsymbol{\epsilon} = \frac{1}{2}(\nabla\mathbf{u}^T + \nabla\mathbf{u}) \quad \Leftrightarrow \quad \epsilon_{hk} = \frac{1}{2}\left(\frac{\partial\, u^h}{\partial\, x^k} + \frac{\partial\, u^k}{\partial\, x^h}\right)
$$

are [9]

$$\begin{cases} \epsilon_{11} = & \frac{1}{2\pi\rho^2}(4\pi a_4 x_1 + 4\pi a_1 {x_1}^2 - h_1 x_2 + 4\pi a_2 x_1 x_2 + k_3 {x_2}^2 + 4\pi a_3 x_1 x_3 - k_2 x_2 x_3) + \\ & + a_1 \log \rho^2 \\ \epsilon_{22} = & \frac{1}{2\pi\rho^2}(h_2 x_1 + k_3 {x_1}^2 + 4\pi b_4 x_2 + 4\pi b_1 x_1 x_2 + 4\pi b_2 {x_2}^2 - k_1 x_1 x_3 + 4\pi b_3 x_2 x_3) + \\ & + b_2 \log \rho^2 \\ \epsilon_{33} = & l_3 \log \rho^2 \\ \epsilon_{12} = & \frac{1}{4\pi\rho^2}((h_1 + 4\pi b_4) x_1 + 4\pi b_1 {x_1}^2 - (h_2 - 4\pi a_4) x_2 - 2(k_3 - 2\pi a_1 - 2\pi b_2) x_1 x_2 + \\ & + 4\pi a_2 {x_2}^2 + (k_2 + 4\pi b_3) x_1 x_3 + (k_1 + 4\pi a_3) x_2 x_3) + \frac{1}{2}(a_2 + b_1) \log \rho^2 \\ \epsilon_{13} = & \frac{1}{4\pi\rho^2}(4\pi l_4 x_1 + 4\pi l_1 {x_1}^2 - h_3 x_2 + (k_2 + 4\pi l_2) x_1 x_2 - k_1 {x_2}^2 + 4\pi l_3 x_1 x_3) + \\ & + \frac{1}{2}(a_3 + l_1) \log \rho^2 \\ \epsilon_{23} = & \frac{1}{4\pi\rho^2}(h_3 x_1 - k_2 {x_1}^2 + 4\pi l_4 x_2 + (k_1 + 4\pi l_1) x_1 x_2 + 4\pi l_2 {x_2}^2 + 4\pi l_3 x_2 x_3) + \\ & + \frac{1}{2}(b_3 + l_2) \log \rho^2 \ . \end{cases} \tag{1.6}$$

In analogy to Volterra's procedure, to calculate the unknown constants $a_1, a_2, a_3, a_4, b_1, b_2, b_3, b_4, l_1, l_2, l_3, l_4$, we have to impose the verification of the indefinite equations of equilibrium and the boundary conditions on the field of displacements. [10]

1.3.1 Constitutive equations

When a homogeneous body, linearly elastic and transversally isotropic, experiences an isotermic displacement at an assigned temperature τ, and departs from its natural state $\mathcal{C}_\tau^*$, then its isotermic strain–energy–function W_τ can be written in the form ([42, 53]

$$W_\tau(\boldsymbol{\epsilon}) = \frac{1}{2}A(\epsilon_{11}^2 + \epsilon_{22}^2) + \frac{1}{2}C\epsilon_{33}^2 + (A - 2N)\epsilon_{11}\epsilon_{22} + F(\epsilon_{11} + \epsilon_{22})\epsilon_{33} + 2L(\epsilon_{23}^2 + \epsilon_{13}^2) + 2N\epsilon_{12}^2$$

(see e.g. [42] p. 160, (16) or [47], Cap. V, §2), where the coefficients A, C, F, L, N are the elastic constants [11] of the cylinder $\mathcal{C}_\tau$ and are, by hypotesis, not vanishing and different from each other.

Given the tensor field of stress $\boldsymbol{\sigma} \equiv ||\sigma_{hk}^{(\tau)}||$ at a temperature τ, the constitutive equations

[9] In engineering practice the *characteristics of strain*, $e_{hk} = \epsilon_{hk}$ if $h = k$, $e_{hk} = 2\epsilon_{hk}$ if $h \neq k$, are usually used (see e.g. [42], Art. 10 p. 39).

[10] It's evident the strain (1.6) proves to be congruent, in that De Saint–Venant's conditions of congruence are automatically verified, independently of the value of the unknown constants.

[11] Being the cylinder is homogeneous, the coefficients A, C, F, L, N are constant.

take the form [12]

$$\sigma_{hh}^{(\tau)} = -\frac{\partial W_\tau}{\partial \epsilon_{hh}} \quad (h = 1, 2, 3) \ , \quad \sigma_{hk}^{(\tau)} = -\frac{1}{2}\frac{\partial W_\tau}{\partial (\epsilon_{hk})} \quad (h, k) = (2, 3), (1, 3), (1, 2) \tag{1.7}$$

(see e.g. [17, 42]).
Writing (1.7) in explicit form, we obtain the Stress-Strain relations:

$$\begin{cases} \sigma_{11}^{(\tau)} = -A\epsilon_{11} - (A - 2N)\epsilon_{22} - F\epsilon_{33}, & \sigma_{12}^{(\tau)} = -2N\epsilon_{12} \\ \sigma_{22}^{(\tau)} = -(A - 2N)\epsilon_{11} - A\epsilon_{22} - F\epsilon_{33}, & \sigma_{13}^{(\tau)} = -2L\epsilon_{13} \\ \sigma_{33}^{(\tau)} = -F(\epsilon_{11} + \epsilon_{22}) - C\epsilon_{33}, & \sigma_{23}^{(\tau)} = -2L\epsilon_{23} \quad . \end{cases} \tag{1.8}$$

Taking into account the relationship between the displacement gradient and the strain tensor, the preceding relations can also be written:

$$\begin{cases} \sigma_{11}^{(\tau)} = -A\dfrac{\partial u_1}{\partial x_1} - (A - 2N)\dfrac{\partial u_2}{\partial x_2} - F\dfrac{\partial u_3}{\partial x_3}, & \sigma_{12}^{(\tau)} = -N\left(\frac{\partial u_1}{\partial x_2} + \frac{\partial u_2}{\partial x_1}\right) \\ \sigma_{22}^{(\tau)} = -A\dfrac{\partial u_2}{\partial x_2} - (A - 2N)\dfrac{\partial u_1}{\partial x_1} - F\dfrac{\partial u_3}{\partial x_3}, & \sigma_{13}^{(\tau)} = -L\left(\frac{\partial u_1}{\partial x_3} + \frac{\partial u_3}{\partial x_1}\right) \\ \sigma_{33}^{(\tau)} = -F\left(\dfrac{\partial u_1}{\partial x_1} + \dfrac{\partial u_2}{\partial x_2}\right) - C\dfrac{\partial u_3}{\partial x_3}, & \sigma_{23}^{(\tau)} = -L\left(\frac{\partial u_2}{\partial x_3} + \frac{\partial u_3}{\partial x_2}\right) \end{cases} \tag{1.9}$$

(see e.g. [17]).
Through the stress–strain relations (1.8) or the preceding equations (1.9), we obtain the following explicit expression of the components of the stress tensor $\boldsymbol{\sigma}$ (relative to the field of

[12] The signs of σ_{hk} are chosen conforming to [47], so a pressure is a positive stress and a tension is a negative stress, as it is usual in theoretical mechanics (see e.g. [48]). Many authors define the stress tensor with the opposite sign from the definition adopted here (see e.g. [42]), as it is almost universal in engineering practice.

displacements (1.4))

$$
\left\{
\begin{aligned}
\sigma_{11}^{(\tau)} = \;& \frac{1}{2\pi\rho^2}(((A-2\,N)\,h_2+4\,\pi\,A\,a_4)\,x_1+(-A\,h_1+4\,\pi\,b_4\,(A-2\,N))\,x_2+((A-2\,N)k_3+\\
&+4\,\pi\,A\,a_1)\,{x_1}^2+4\,\pi(\,A\,a_2+(A\,-2\,N)\,b_1)\,x_1\,x_2+(A\,k_3-\,\pi\,(N-\,A)\,b_2)\,{x_2}^2+\\
&+((2\,N-A)\,k_1+4\,\pi\,A\,a_3)\,x_1\,x_3+(-A\,k_2+4\,\pi(\,A-2\,N\,)\,b_3)\,x_2\,x_3)+\\
&-(Aa_1+(2N-A)b2+Fl_3)\log\rho^2\\
\sigma_{22}^{(\tau)} = \;& -\frac{1}{2\pi\rho^2}\,(A\,h_2+4\,a_4\;(A-2\,N)\;\pi)\;x_1+4\,a_1\;(A-2\,N)\;\pi\,{x_1}^2+(h_1\,(-A+2\,N)+\\
&+4\,A\,b_4\,\pi)\,x_2+4\;(A\,b_1+a_2\;(A-2\,N))\;\pi\,x_1\,x_2-2\,(k_3\,N-2\,A\,b_2\,\pi)\,{x_2}^2+\\
&+(-A\,k_1+4\,a_3\;(A-2\,N)\;\pi)\;x_1\,x_3+(k_2\;(-A+2\,N)+4\,A\,b_3\,\pi)\;x_2\,x_3)-\frac{k_3}{2\,\pi}\,A+\\
&-(A\,b_2+F\,l_3+a_1\;(A-2\,N))\;\log\rho^2\\
\sigma_{33}^{(\tau)} = \;& -F\frac{k_3}{2\pi}-\frac{F}{2\pi\rho^2}((h_2+4\,a_4\,\pi)\;x_1+4\,a_1\,\pi\,{x_1}^2+(-h_1+4\,b_4\,\pi)\;x_2+4\;(a_2+b_1)\;\pi\,x_1\,x_2+\\
&+4\,b_2\,\pi\,{x_2}^2\,(-k_1+4\,a_3\,\pi)\;x_1\,x_3+(-k_2+4\,b_3\,\pi)\;x_2\,x_3)-(F\;(a_1+b_2)+C\,l_3)\;\log\rho^2\\
\sigma_{12}^{(\tau)} = \;& -\frac{N}{2\pi\rho^2}((h_1+4\,b_4\,\pi)\,x_1+4\,b_1\,\pi\,{x_1}^2+(-h_2+4\,a_4\,\pi)\,x_2+(-2\,k_3+4\,a_1\,\pi+\\
&+4\,b_2\,\pi)\,x_1\,x_2+4\,a_2\,\pi\,{x_2}^2+(k_2+4\,b_3\,\pi)\,x_1\,x_3+(k_1+4\,a_3\,\pi)\,x_2\,x_3)+\\
&-(a_2+b_1)\,N\;\log\rho^2\\
\sigma_{13}^{(\tau)} = \;& -\frac{L}{2\pi\rho^2}\left(4\,l_4\,\pi\,x_1+4\,l_1\,\pi\,{x_1}^2-h_3\,x_2+(k_2+4\,l_2\,\pi)\;x_1\,x_2-k_1\,{x_2}^2+4\,l_3\,\pi\,x_1\,x_3\right)+\\
&-L\;(a_3+l_1)\;\log\rho^2\\
\sigma_{23}^{(\tau)} = \;& -\frac{L}{2\pi\rho^2}\left(h_3\,x_1-k_2\,{x_1}^2+4\,l_4\,\pi\,x_2+(k_1+4\,l_1\,\pi)x_1\,x_2+4\,l_2\,\pi\,{x_2}^2+4\,l_3\,\pi\,x_2\,x_3\right)+\\
&-L\;(b_3+l_2)\;\log\rho^2
\end{aligned}
\right. \tag{1.10}
$$

Remark Being the cylinder is transversally isotropic, the stress-strain relations (1.8) are invariant with respect to the exchange of the axes x_1 and x_2. We can obtain from (1.8),(1.10) the stress-strain relations for a homogeneous and isotropic cylinder by making them invariant with respect to the exchange of any pair of axes or to the directional change of any one of the axes (see e.g. [42], p. 102). The five elastic constants therefore, must verify the following three conditions of isotropy:

$$C = A \;\;, \qquad L = N \;\;, \qquad F = A - 2N \tag{1.11}$$

which reduce the independent elastic constants to only A and N.

1.3.2 Indefinite equations

In that $\mathcal{C}$ is initially found in a natural state, Cauchy's static equations, in absence of force of mass, must be verified:

$$\operatorname{div}\boldsymbol{\sigma} = 0\;, \qquad \forall P^* \in \mathcal{C}_\tau^* \tag{1.12}$$

If (1.12) is projected onto the axes, and expressions (1.9) of the stress–tensor are taken into account, we obtain:

$$A\frac{\partial^2 u_1}{(\partial x_1)^2}+N\frac{\partial^2 u_1}{(\partial x_2)^2}+L\frac{\partial^2 u_1}{(\partial x_3)^2}+(A-N)\frac{\partial^2 u_2}{\partial x_1\partial x_2}+(F+L)\frac{\partial^2 u_3}{\partial x_1\partial x_3}=0 \qquad (1.13)$$

$$N\frac{\partial^2 u_2}{(\partial x_1)^2}+A\frac{\partial^2 u_2}{(\partial x_2)^2}+L\frac{\partial^2 u_2}{(\partial x_3)^2}+(A-N)\frac{\partial^2 u_1}{\partial x_1\partial x_2}+(F+L)\frac{\partial^2 u_3}{\partial x_2\partial x_3}=0 \qquad (1.14)$$

$$L\frac{\partial^2 u_3}{(\partial x_1)^2}+L\frac{\partial^2 u_3}{(\partial x_2)^2}+C\frac{\partial^2 u_3}{(\partial x_3)^2}+(F+L)\frac{\partial^2 u_1}{\partial x_1\partial x_3}+(F+L)\frac{\partial^2 u_2}{\partial x_2\partial x_3}=0 \qquad (1.15)$$

(see e.g. [17]).
Referring to (1.15) or the expressions of stress (1.10), the equations of equilibrium (1.12) can be written in the explicit forms:

$$\left\{\begin{array}{ll}(\mathrm{div}\,\boldsymbol{\sigma})_1= & \frac{1}{2\pi\rho^4}((A-N)(4\pi a_4+h_2){x_1}^2+2(A-N)(4\pi b_4-h_1)x_1x_2+\\ & -(A-N)(4\pi a_4+h_2){x_2}^2-2(2\pi a_1(A+N)+2\pi(A-N)b_2-Nk_3+\\ & +2\pi(F+L)l_3){x_1}^3-4\pi((3N-A)a_2-(A-N)b_1){x_1}^2x_2+\\ & +(A-N)(4\pi a_3-k_1){x_1}^2x_3+2(2\pi(N-3A)a_1+2\pi(A-N)b_2+Nk_3+\\ & -2\pi(F+L)l_3)x_1{x_2}^2+2(A-N)(4\pi b_3-k_2)x_1x_2x_3-4\pi((A+N)a_2+\\ & +(A-N)b_1){x_2}^3-(A-N)(4\pi a_3-k_1){x_2}^2x_3)=0\end{array}\right. \qquad (1.16)$$

$$\left\{\begin{array}{ll}(\mathrm{div}\,\boldsymbol{\sigma})_2= & \frac{1}{2\pi\rho^4}((A-N)(h_1-4\pi b_4){x_1}^2+2(A-N)(h_2+4\pi a_4)x_1x_2+(A-N)(4\pi b_4+\\ & -h_1){x_2}^2-4\pi((A-N)a_2+(A+N)b_1){x_1}^3+2(2\pi(A-N)a_1+2\pi(-3A+\\ & +N)b_2+Nk_3-2\pi(F+L)l_3){x_1}^2x_2+(A-N)(k_2-4\pi b_3){x_1}^2x_3+\\ & +4\pi((A-N)a_2+(A-3N)b_1)x_1{x_2}^2+2(A-N)(4\pi a_3-k_1)x_1x_2x_3+\\ & -2(2\pi(A-N)a_1+2\pi(A+N)b_2-Nk_3+2\pi(F+L)l_3){x_2}^3+\\ & -(A-N)(4\pi b_3-k_2){x_2}^2x_3)=0\end{array}\right. \qquad (1.17)$$

$$\left\{\begin{array}{ll}(\mathrm{div}\,\boldsymbol{\sigma})_3= & -\frac{1}{2\pi\rho^2}((4\pi(F+L)a_3+(L-F)k_1+8\pi Ll_1)x_1+(4\pi(F+L)b_3+\\ & +(L-F)k_2+8\pi Ll_2)x_2)=0\end{array}\right. \qquad (1.18)$$

If we make the coefficients of the various monomials $(x_1)^j(x_2)^k(x_3)^l$ equal to zero, we arrive at a system of linear equations, not all independent, for the unknowns a_h, b_h, l_h $(h=1,2,3,4)$. By annulling the coefficients of the monomials $x_1^2x_3$ (or $x_2^2x_3$), x_1^2 (or x_2^2), $x_1x_2x_3$, x_1x_2, in (1.16) (or in (1.17)) we find respectively (in the aforementioned hypothesis $A\neq N$)

$$a_3=\frac{k_1}{4\pi}\ ;\quad a_4=-\frac{h_2}{4\pi}\ ;\quad b_3=\frac{k_2}{4\pi}\ ;\quad b_4=\frac{h_1}{4\pi} \qquad (1.19)$$

If we annul the coefficients of the monomials $x_1^2x_2$, x_2^3 in (1.16) (or the coefficients of the monomials $x_1x_2^2$, x_1^3 in (1.17)), we obtain the homogeneous system

$$\begin{cases} (3N-A)a_2+(N-A)b_1=0 \\ (N+A)a_2+(N-A)b_1=0 \end{cases}$$

where the only solution is $a_2=0\ ,\ b_1=0$ (in the same hypothesis $A\neq N$).
If we annul the coefficient of x_1 in (1.18), we obtain the equation

$$4\pi(F+L)a_3-(F-L)k_1+8\pi Ll_1=0\ .$$

And if we take into account the calculated value of a_3, we find $l_1=-\dfrac{k_1}{4\pi}$.
By annulling the coefficient of x_2 in (1.18), we obtain the equation

$$4\pi(F+L)b_3-(F-L)k_2+8\pi Ll_2=0\ .$$

And by taking into account the calculated value of b_3, we find $l_2=-\dfrac{k_2}{4\pi}$.
Finally, by annulling the coefficients of the monomials x_1^3, $x_1x_2^2$ in (1.16) and the coefficients of the monomials x_2^3, $x_1^2x_2$ in (1.17), we obtain the following subsystem of four linear equations in the three unknowns a_1, b_2, l_3

$$\begin{cases} 2\pi[(A+N)a_1+(A-N)b_2+(F+L)l_3]=Nk_3 \\ 2\pi(3A-N)a_1-2\pi(A-N)b_2+2\pi(F+L)l_3=Nk_3 \\ 2\pi(A-N)a_1+2\pi(A+N)b_2+2\pi(F+L)l_3=Nk_3 \\ 2\pi(N-A)a_1+2\pi(3A-N)b_2+2\pi(F+L)l_3=Nk_3 \end{cases} \tag{1.20}$$

which has the ∞^1 solutions [13]

$$b_2=a_1\quad ,\qquad l_3=\frac{Nk_3-4\pi Aa_1}{2\pi(F+L)}\ . \tag{1.21}$$

In summary we can say that the displacement (1.3) satisfies the indefinite equations of elastic equilibrium, and therefore can be considered as an elastic displacement in an equilibrium problem if the following conditions are verified (and $A\neq N$):

$$\begin{cases} a_2=0\ ;\quad a_3=\dfrac{k_1}{4\pi}\ ;\quad a_4=-\dfrac{h_2}{4\pi}; \\ b_1=0\ ;\quad b_2=a_1\ ;\quad b_3=\dfrac{k_2}{4\pi}\ ;\quad b_4=\dfrac{h_1}{4\pi}\ ; \\ l_1=-a_3=-\dfrac{k_1}{4\pi}\ ;\quad l_2=-b_3=-\dfrac{k_2}{4\pi}\ ;\quad l_3=\dfrac{Nk_3-4\pi Aa_1}{2\pi(F+L)}\ , \end{cases} \tag{1.22}$$

while the constants a_1 and l_4 are still undetermined.

[13] It is sufficient to consider any two of (1.20) to obtain $(1.21)_1$. Therefore (1.20) reduce to the unique equation $4\pi Aa_1-Nk_3+2\pi(F+L)l_3=0$.

So the cartesian components of the displacement (1.3), which satisfy the indefinite equations (1.12), take the form

$$\begin{cases} u_1 = \dfrac{1}{2\pi}(h_1 - k_3x_2 + k_2x_3)\,\theta + \left(-\dfrac{h_2}{4\pi} + \dfrac{k_1}{4\pi}x_3 + a_1x_1\right)\log\rho^2 \\ u_2 = \dfrac{1}{2\pi}(h_2 + k_3x_1 - k_1x_3)\,\theta + \left(\dfrac{h_1}{4\pi} + \dfrac{k_2}{4\pi}x_3 + a_1x_2\right)\log\rho^2 \\ u_3 = \dfrac{1}{2\pi}(h_3 - k_2x_1 + k_1x_2)\,\theta - \left(\dfrac{k_1}{4\pi}x_1 + \dfrac{k_2}{4\pi}x_2 - l_3x_3 - l_4\right)\log\rho^2 \end{cases} \tag{1.23}$$

where l_3 has the expression (1.21).

Deformation, stress and forces on the boundary

If (1.23) are introduced into (1.6), we find the following expression for strain tensor, relative to the vector field of displacements (1.23)

$$\begin{cases} \epsilon_{11} = \dfrac{1}{2\pi\rho^2}(-h_2x_1 - h_1x_2 + 4\pi a_1{x_1}^2 + k_3{x_2}^2 + k_1x_1x_3 - k_2x_2x_3) + a_1\log\rho^2 \\ \epsilon_{22} = \dfrac{1}{2\pi\rho^2}(h_2x_1 + h_1x_2 + 4\pi a_1{x_2}^2 + k_3{x_1}^2 - k_1x_1x_3 + k_2x_2x_3) + a_1\log\rho^2 \\ \epsilon_{33} = l_3\log\rho^2 \\ \epsilon_{12} = \dfrac{1}{2\pi\rho^2}(h_1x_1 - h_2x_2 - (k_3 - 4\pi a_1)x_1x_2 + k_2x_1x_3 + k_1x_2x_3) \\ \epsilon_{13} = \dfrac{1}{4\pi\rho^2}(4\pi l_4x_1 - h_3x_2 + 4\pi l_3x_1x_3) - \dfrac{k_1}{4\pi} \\ \epsilon_{23} = \dfrac{1}{4\pi\rho^2}(4\pi l_4x_2 + h_3x_1 + 4\pi l_3x_2x_3) - \dfrac{k_2}{4\pi}\ . \end{cases} \tag{1.24}$$

If (1.24) are substituted into (1.10), which express the components of the stress tensor by those of the tensor of deformation, we obtain the stress which satisfies Cauchy's equations of

equilibrium (1.12):

$$\begin{cases} \sigma_{11}^{(\tau)} = & \frac{N}{\pi\rho^2}\left(h_2x_1 + h_1x_2 + k_3{x_1}^2 + 4\pi a_1{x_2}^2 - k_1x_1x_3 + k_2x_2x_3\right) + \\ & -\frac{A}{2\pi}\left(k_3 + 4\pi a_1\right) + \left[2a_1(N-A) - Fl_3\right]\log\rho^2 \\ \sigma_{22}^{(\tau)} = & \frac{N}{\pi\rho^2}\left(-h_2x_1 - h_1x_2 + k_3{x_2}^2 + 4\pi a_1{x_1}^2 + k_1x_1x_3 - k_2x_2x_3\right) + \\ & -\frac{A}{2\pi}\left(k_3 + 4\pi a_1\right) + \left[2a_1(N-A) - Fl_3\right]\log\rho^2 \\ \sigma_{33}^{(\tau)} = & -\frac{F}{2\pi}\left(k_3 + 4\pi a_1\right) - \left(2Fa_1 - Cl_3\right)\log\rho^2 \\ \sigma_{12}^{(\tau)} = & \frac{N}{\pi\rho^2}\left[-h_1x_1 + h_2x_2 + (k_3 - 4\pi a_1)x_1x_2 - k_2x_1x_3 - k_1x_2x_3\right] \\ \sigma_{13}^{(\tau)} = & \frac{L}{2\pi\rho^2}\left(h_3x_2 - 4\pi l_4x_1 - 4\pi l_3x_1x_3\right) + \frac{Lk_1}{2\pi} \\ \sigma_{23}^{(\tau)} = & \frac{L}{2\pi\rho^2}\left(-h_3x_1 - 4\pi l_4x_2 - 4\pi l_3x_2x_3\right) + \frac{Lk_2}{2\pi} \end{cases} \tag{1.25}$$

Boundary conditions

Finally boundary conditions must be verified:

$$\boldsymbol{\sigma}\cdot\mathbf{n} - \mathbf{f} = \mathbf{0} \quad \Longleftrightarrow \quad \sigma_{h_1}n_1 + \sigma_{h_2}n_2 + \sigma_{h_3}n_3 = f_h \quad (h = 1,2,3) \qquad \forall Q^* \in \partial\mathcal{C}_\tau^* \,, \tag{1.26}$$

where $\mathbf{f}(\mathbf{Q}^*)$ are the vectorial surface forces and $\mathbf{n} \equiv (n_1, n_2, n_3)$ is the unitary vector normal to $\partial\mathcal{C}_\tau^*$, with an internal orientation.

To calculate the forces which we must apply on the boundary of the cylinder to determine the principal displacement (1.23), we divide the boundary $\partial\mathcal{C}_\tau^*$ into the parts ${\Sigma^*}_1$, ${\Sigma^*}_2$, ${\alpha^*}_1$ and ${\alpha^*}_2$. By taking into account (1.25) and projecting (1.26) onto the axes, we obtain four groups of equations.
First we consider the boundary conditions on the two lateral surfaces:
1) on ${\Sigma^*}_1$ ($\mathbf{n} = \mathbf{c_1}\cos\theta + \mathbf{c_2}\sin\theta$, $x_1 = r\cos\theta,\ x_2 = r\sin\theta,\ 0 \le x_3 \le d$)

$$\begin{cases} \left[\sigma_{11}^{(\tau)}\cos\theta + \sigma_{12}^{(\tau)}\sin\theta\right]_{{\Sigma^*}_1} = & \frac{1}{2\pi r}[2Nh_2 + ((2N-A)k_3 - 4\pi Aa_1)x_1 - 2Nk_1x_3 + \\ & +4\pi(N-A)a_1x_1\log\rho^2 - 2\pi Fl_3x_1\log\rho^2]_{{\Sigma^*}_1} = (f_1)_{{\Sigma^*}_1} \\ \left[\sigma_{12}^{(\tau)}\cos\theta + \sigma_{22}^{(\tau)}\sin\theta\right]_{{\Sigma^*}_1} = & \frac{1}{2\pi r}[-2Nh_1 + ((2N-A)k_3 - 4\pi Aa_1)x_2 - 2Nk_2x_3 + \\ & +4\pi(N-A)a_1x_2\log\rho^2 - 2\pi Fl_3x_2\log\rho^2]_{{\Sigma^*}_1} = (f_2)_{{\Sigma^*}_1} \\ \left[\sigma_{13}^{(\tau)}\cos\theta + \sigma_{23}^{(\tau)}\sin\theta\right]_{{\Sigma^*}_1} = & \frac{L}{2\pi r}[-4\pi l_4 + k_1x_1 + k_2x_2 - 4\pi l_3x_3] = (f_3)_{{\Sigma^*}_1} \end{cases} \tag{1.27}$$

2) on $\Sigma^*{}_2$ ($\mathbf{n} = -\mathbf{c_1}\cos\theta - \mathbf{c_2}\sin\theta, \quad x_1 = R\cos\theta,\ x_2 = R\sin\theta,\ 0 \le x_3 \le d$)

$$\begin{cases} \left[-\sigma_{11}^{(\tau)}\cos\theta - \sigma_{12}^{(\tau)}\sin\theta\right]_{\Sigma^*{}_2} = & \frac{1}{2\pi R}[-2Nh_2 - ((2N-A)k_3 - 4\pi a_1)x_1 + 2Nk_1x_3 + \\ & -4\pi(N-A)a_1x_1\log\rho^2 + 2\pi Fl_3x_1\log\rho^2]_{\Sigma^*{}_2} = (f_1)_{\Sigma^*{}_2} \\ \left[-\sigma_{12}^{(\tau)}\cos\theta - \sigma_{22}^{(\tau)}\sin\theta\right]_{\Sigma^*{}_2} = & \frac{1}{2\pi R}[2Nh_1 - ((2N-A)k_3 - 4\pi a_1)x_2 + 2Nk_2x_3 + \\ & -4\pi(N-A)a_1x_2\log\rho^2 + 2\pi Fl_3x_2\log\rho^2]_{\Sigma^*{}_2} = (f_2)_{\Sigma^*{}_2} \\ \left[-\sigma_{13}^{(\tau)}\cos\theta - \sigma_{23}^{(\tau)}\sin\theta\right]_{\Sigma^*{}_2} = & \frac{L}{2\pi R}[4\pi l_4 - k_1x_1 - k_2x_2 + 4\pi l_3x_3] = (f_3)_{\Sigma^*{}_2} \end{cases} \tag{1.28}$$

We can divide the surface forces (1.27)–(1.28) applied on $\Sigma^*{}_1$ and on $\Sigma^*{}_2$ into the following vector fields, all equivalent to zero:

i) $\left\{P^*, \mathbf{f}^{(1)\prime}(P^*)\mathrm{d}\,\Sigma^*{}_1\right\}_{\Sigma^*{}_1}$, consisting of couples of zero arms and so equivalent to zero, in fact

$$\begin{cases} \left[f_1^{(1)\prime}(x_1,x_2,x_3)\right]_{\Sigma^*{}_1} = & \frac{1}{2\pi r}\left[((2N-A)k_3 - 4\pi Aa_1)x_1 - 2Nk_1x_3 + 4\pi(N-A)a_1x_1\log\rho^2 + \right. \\ & \left. -2\pi Fl_3x_1\log\rho^2\right]_{\Sigma^*{}_1} = -\left[f_1^{(1)\prime}(-x_1,-x_2,x_3)\right]_{\Sigma^*{}_1} \\ \left[f_2^{(1)\prime}(x_1,x_2,x_3)\right]_{\Sigma^*{}_1} = & \frac{1}{2\pi r}\left[((2N-A)k_3 - 4\pi Aa_1)x_2 - 2Nk_2x_3 + 4\pi(N-A)a_1x_2\log\rho^2 + \right. \\ & \left. -2\pi Fl_3x_2\log\rho^2\right]_{\Sigma^*{}_1} = -\left[f_2^{(1)\prime}(-x_1,-x_2,x_3)\right]_{\Sigma^*{}_1} \\ \left[f_3^{(1)\prime}(x_1,x_2,x_3)\right]_{\Sigma^*{}_1} = & \frac{L}{2\pi r}\left[-4\pi l_4 + k_1x_1 + k_2x_2 - 4\pi l_3x_3\right] = -\left[f_3^{(1)\prime}(-x_1,-x_2,x_3)\right]_{\Sigma^*{}_1}; \end{cases}$$

ii) $\left\{P^*, \mathbf{f}^{(2)\prime}(P^*)\mathrm{d}\,\Sigma^*{}_2\right\}_{\Sigma^*{}_2}$, which, analogously, consists of couples of zero arms.

iii) The pair of two constant vector fields, parallel and opposite, $\left\{\mathbf{f}^{(1)\prime\prime}\mathrm{d}\,\Sigma^*{}_1\right\}_{\Sigma^*{}_1} \equiv \left\{\mathbf{f}^{(1)\prime\prime}2\pi r\mathrm{d}\,x_3\right\}_{\Sigma^*{}_1}$ and $\left\{\mathbf{f}^{(2)\prime\prime}\mathrm{d}\,\Sigma^*{}_2\right\}_{\Sigma^*{}_2} \equiv \left\{\mathbf{f}^{(2)\prime\prime}2\pi R\mathrm{d}\,x_3\right\}_{\Sigma^*{}_2}$

$$\begin{cases} (f_1^{(1)})''_{\Sigma^*{}_1}\mathrm{d}\,\Sigma^*{}_1 = 2Nh_2\mathrm{d}\,x_3\ , \quad (f_2^{(1)})''_{\Sigma^*{}_1}\mathrm{d}\,\Sigma^*{}_1 = -2Nh_1\mathrm{d}\,x_3\ , \quad (f_3^{(1)})''_{\Sigma^*{}_1}\mathrm{d}\,\Sigma^*{}_1 = -4\pi Ll_4\mathrm{d}\,x_3 \\ (f_1^{(2)})''_{\Sigma^*{}_2}\mathrm{d}\,\Sigma^*{}_2 = -2Nh_2\mathrm{d}\,x_3\ , \quad (f_2^{(2)})''_{\Sigma^*{}_2}\mathrm{d}\,\Sigma^*{}_2 = 2Nh_1\mathrm{d}\,x_3\ , \quad (f_3^{(2)})''_{\Sigma^*{}_2}\mathrm{d}\,\Sigma^*{}_2 = 4\pi Ll_4\mathrm{d}\,x_3 \end{cases} \tag{1.29}$$

that together have, by symmetry, their center coincident with the center of the cylinder, and are equivalent to their resultant applied to the center. Since their two resultants $\mathbf{r}''_{(1)}$ and $\mathbf{r}''_{(2)}$ are [14]

$$\begin{cases} r_1^{(1)\prime\prime} = 2Nh_2d\ , \quad r_2^{(1)\prime\prime} = -2Nh_1d\ , \quad r_3^{(1)\prime\prime} = -4\pi Ll_4d \\ r_1^{(2)\prime\prime} = -2Nh_2d\ , \quad r_2^{(2)\prime\prime} = 2Nh_1d\ , \quad r_3^{(2)\prime\prime} = 4\pi Ll_4d \end{cases} \tag{1.30}$$

[14] $\mathbf{r}^{(1)\prime\prime} = \int_{\Sigma^*{}_1}\mathbf{f}^{(1)\prime\prime}\mathrm{d}\Sigma_1^* = \mathbf{f}^{(1)\prime\prime}2\pi rd \quad , \qquad \mathbf{r}^{(2)\prime\prime} = \int_{\Sigma^*{}_2}\mathbf{f}^{(2)\prime\prime}\mathrm{d}\Sigma_2^* = \mathbf{f}^{(2)\prime\prime}2\pi Rd\ .$

it is obvious that, being $\mathbf{r}''_{(1)} + \mathbf{r}''_{(2)} = \mathbf{0}$, also the vector field $\{(P^*, \mathbf{f}^{(1)''})_{\Sigma^*{}_1}, (P^*, \mathbf{f}^{(2)''})_{\Sigma^*{}_2}\}$ is equivalent to a couple of zero arm.

Finally we consider the boundary conditions on the two bases:

3) on $\alpha^*{}_1$ ($\mathbf{n} = \mathbf{c_3} \equiv (0,0,1)$, $x_3 = 0$)

$$\begin{cases} [\sigma^{(\tau)}_{13}]_{\alpha^*{}_1} = \dfrac{L}{2\pi}\left[k_1 + \dfrac{1}{\rho^2}(h_3 x_2 - 4\pi l_4 x_1)\right]_{\alpha^*{}_1} = (f_1)_{\alpha^*{}_1} \\ [\sigma^{(\tau)}_{23}]_{\alpha^*{}_1} = \dfrac{L}{2\pi}\left[k_2 - \dfrac{1}{\rho^2}(h_3 x_1 + 4\pi l_4 x_2)\right]_{\alpha^*{}_1} = (f_2)_{\alpha^*{}_1} \\ [\sigma^{(\tau)}_{33}]_{\alpha^*{}_1} = \left[\dfrac{F}{2\pi}(k_3 + 4\pi a_1) + (2Fa_1 + Cl_3)\log\rho^2\right]_{\alpha^*{}_1} = (f_3)_{\alpha^*{}_1} \end{cases} \tag{1.31}$$

4) on $\alpha^*{}_2$ ($\mathbf{n} = -\mathbf{c_3} \equiv (0,0,-1)$, $x_3 = d$)

$$\begin{cases} [-\sigma^{(\tau)}_{13}]_{\alpha^*{}_2} = -\dfrac{L}{2\pi}\left[k_1 + \dfrac{1}{\rho^2}\left(h_3 x_2 - 4\pi(l_3 d + l_4)x_1\right)\right]_{\alpha^*{}_2} = (f_1)_{\alpha^*{}_2} \\ [-\sigma^{(\tau)}_{23}]_{\alpha^*{}_2} = -\dfrac{L}{2\pi}\left[k_2 - \dfrac{1}{\rho^2}\left(h_3 x_1 + 4\pi(l_3 d + l_4)x_2\right)\right]_{\alpha^*{}_2} = (f_2)_{\alpha^*{}_2} \\ [-\sigma^{(\tau)}_{33}]_{\alpha^*{}_2} = -\left[\dfrac{F}{2\pi}(k_3 + 4\pi a_1) + (2Fa_1 + Cl_3)\log\rho^2\right]_{\alpha^*{}_2} = (f_3)_{\alpha^*{}_2} \end{cases} \tag{1.32}$$

Also the surface forces exerting on the two bases must be equivalent to zero. So, taking into consideration (1.31),(1.32), we must put

$$l_3 = 0 \ , \tag{1.33}$$

and consequently we obtain from (1.21)

$$a_1 = \frac{N}{A}\frac{k_3}{4\pi} \ . \tag{1.34}$$

Condition (1.33) together with (1.34) must be verified so that the surface forces corresponding to the dislocation are equivalent to zero, therefore l_3 and a_1 are not arbitrary.

1.3.3 Vector field of displacements

From (1.33)–(1.34) we can now write the definitive expression of the vector field of displacements (1.23)

$$\begin{cases} u_1 = \dfrac{1}{2\pi}\left\{(h_1 - k_3 x_2 + k_2 x_3)\,\theta + \dfrac{1}{2}\left(-h_2 + k_1 x_3 + \dfrac{N}{A}k_3 x_1\right)\log\rho^2\right\} \\ u_2 = \dfrac{1}{2\pi}\left\{(h_2 + k_3 x_1 - k_1 x_3)\,\theta + \dfrac{1}{2}\left(h_1 + k_2 x_3 + \dfrac{N}{A}k_3 x_2\right)\log\rho^2\right\} \\ u_3 = \dfrac{1}{2\pi}\left\{(h_3 - k_2 x_1 + k_1 x_2)\,\theta - \dfrac{1}{2}\left(k_1 x_1 + k_2 x_2 - 4\pi l_4\right)\log\rho^2\right\} \end{cases} \tag{1.35}$$

These formulas demonstrate that the vector field of displacements depends exclusively on the ratio N/A of only two of the five elastic constants which characterize a transversally isotropic elastic body.

Remark If we impose the isotropy conditions (1.11) on the five elastic constants, and we put $A = \lambda + 2\mu$, $N = \mu$ and $l_4 = 0$, we once again obtain from (1.35) Volterra's formulas (1.2) relative to the isotropic case.

1.3.4 Deformation, stress and surface forces corresponding to the established displacement

If we substitute the values $l_3 = 0$ and $a_1 = \dfrac{N}{A}\dfrac{k_3}{4\pi}$ in (1.5), in (1.24), in (1.25) and in (1.27)–(1.32), we obtain the following explicit definitive expressions (corresponding to the displacement (1.35)):
1) for the gradient of displacement $\nabla\mathbf{u}$

$$\begin{cases}
\dfrac{\partial u_1}{\partial x_1} = & \dfrac{1}{2\pi\rho^2}(-h_2\,x_1 - h_1\,x_2 + \dfrac{N}{A}\,k_3\,{x_1}^2 + k_3\,{x_2}^2 + k_1\,x_1\,x_3 - k_2\,x_2\,x_3) + \dfrac{N}{A}\,\dfrac{k_3}{4\,\pi}\,\log\rho^2 \\
\dfrac{\partial u_1}{\partial x_2} = & \dfrac{1}{2\pi\rho^2}\left(h_1\,x_1 - h_2\,x_2 + \left(\dfrac{N}{A} - 1\right)k_3\,x_1\,x_2 + k_2\,x_1\,x_3 + k_1\,x_2\,x_3\right) - \dfrac{k_3}{2\,\pi}\,\theta \\
\dfrac{\partial u_1}{\partial x_3} = & \dfrac{k_2}{2\pi}\theta + \dfrac{k_1}{4\pi}\log\rho^2 \\
\dfrac{\partial u_2}{\partial x_1} = & \dfrac{1}{2\pi\rho^2}\left(h_1\,x_1 - h_2\,x_2 + \left(\dfrac{N}{A} - 1\right)\,k_3\,x_1\,x_2 + k_2\,x_1\,x_3 + k_1\,x_2\,x_3\right) + \dfrac{k_3}{2\pi}\,\theta \\
\dfrac{\partial u_2}{\partial x_2} = & \dfrac{1}{2\pi\rho^2}(h_2\,x_1 + h_1\,x_2 + \dfrac{N}{A}\,k_3\,{x_2}^2 + k_3\,{x_1}^2 - k_1\,x_1\,x_3 + k_2\,x_2\,x_3) + \dfrac{N}{A}\,\dfrac{k_3}{4\,\pi}\,\log\rho^2 \\
\dfrac{\partial u_2}{\partial x_3} = & -\dfrac{k_1}{2\pi}\theta + \dfrac{k_2}{4\,\pi}\,\log\rho^2 \\
\dfrac{\partial u_3}{\partial x_1} = & \dfrac{1}{2\pi\rho^2}(4\,\pi\,l_4\,x_1 - h_3\,x_2 - k_1\,{x_1}^2 - k_1\,{x_2}^2) - \dfrac{k_2}{2\pi}\theta + \dfrac{k_1}{4\pi}\log\rho^2 \\
\dfrac{\partial u_3}{\partial x_2} = & \dfrac{1}{2\pi\rho^2}(4\,\pi\,l_4\,x_2 + h_3\,x_1 - k_2\,{x_1}^2 - k_2\,{x_2}^2) + \dfrac{k_1}{2\pi}\theta - \dfrac{k_2}{4\pi}\log\rho^2 \\
\dfrac{\partial u_3}{\partial x_3} = & 0
\end{cases} \tag{1.36}$$

2) for the tensor field of strain

$$\begin{cases} \epsilon_{11} = \dfrac{1}{2\pi\rho^2}\left(-h_2x_1 - h_1x_2 + \dfrac{N}{A}k_3{x_1}^2 + k_3{x_2}^2 + k_1x_1x_3 - k_2x_2x_3\right) + \dfrac{N}{A}\dfrac{k_3}{4\pi}\log\rho^2 \\ \epsilon_{22} = \dfrac{1}{2\pi\rho^2}\left(h_2x_1 + h_1x_2 + \dfrac{N}{A}k_3{x_2}^2 + k_3{x_1}^2 - k_1x_1x_3 + k_2x_2x_3\right) + \dfrac{N}{A}\dfrac{k_3}{4\pi}\log\rho^2 \\ \epsilon_{33} = 0 \\ \epsilon_{12} = \dfrac{1}{2\pi\rho^2}\left(h_1x_1 - h_2x_2 + \left(\dfrac{N}{A} - 1\right)k_3x_1x_2 + k_2x_1x_3 + k_1x_2x_3\right) \\ \epsilon_{13} = \dfrac{1}{4\pi\rho^2}(4\pi l_4x_1 - h_3x_2) - \dfrac{k_1}{4\pi} \\ \epsilon_{23} = \dfrac{1}{4\pi\rho^2}(4\pi l_4x_2 + h_3x_1) - \dfrac{k_2}{4\pi} \end{cases} \tag{1.37}$$

3) for the tensor field of stress

$$\begin{cases} \sigma_{11}^{(\tau)} = & \dfrac{N}{\pi\rho^2}\left(h_2x_1 + h_1x_2 + \dfrac{N}{A}k_3{x_2}^2 + k_3{x_1}^2 - k_1x_1x_3 + k_2x_2x_3\right) + \\ & -(N+A)\dfrac{k_3}{2\pi} + (N-A)\dfrac{N}{A}\dfrac{k_3}{2\pi}\log\rho^2 \\ \sigma_{22}^{(\tau)} = & -\dfrac{N}{\pi\rho^2}\left(h_2x_1 - h_1x_2 + \dfrac{N}{A}k_3{x_1}^2 + k_3{x_2}^2 + k_1x_1x_3 - k_2x_2x_3\right) + \\ & -(N+A)\dfrac{k_3}{2\pi} + (N-A)\dfrac{N}{A}\dfrac{k_3}{2\pi}\log\rho^2 \\ \sigma_{33}^{(\tau)} = & -F\left(\dfrac{N}{A} + 1\right)\dfrac{k_3}{2\pi} - F\dfrac{N}{A}\dfrac{k_3}{2\pi}\log\rho^2 \\ \sigma_{12}^{(\tau)} = & \dfrac{N}{\pi\rho^2}\left(-h_1x_1 + h_2x_2 - \left(\dfrac{N}{A} - 1\right)k_3x_1x_2 - k_2x_1x_3 - k_1x_2x_3\right) \\ \sigma_{13}^{(\tau)} = & -\dfrac{L}{2\pi\rho^2}(4\pi l_4x_1 - h_3x_2) + \dfrac{Lk_1}{2\pi} \\ \sigma_{23}^{(\tau)} = & -\dfrac{L}{2\pi\rho^2}(4\pi l_4x_2 + h_3x_1) + \dfrac{Lk_2}{2\pi} \end{cases} \tag{1.38}$$

4) for the surface forces, respectively on:

$$\Sigma^*{}_1 \qquad \begin{cases} (f_1)_{\Sigma^*{}_1} = & \dfrac{1}{2\pi r}\left[2Nh_2 + \left(\dfrac{N}{A} - 1\right)(A + N\log\rho^2)k_3x_1 - 2Nk_1x_3\right]_{\Sigma^*{}_1} \\ (f_2)_{\Sigma^*{}_1} = & \dfrac{1}{2\pi r}\left[-2Nh_1 + \left(\dfrac{N}{A} - 1\right)(A + N\log\rho^2)k_3x_2 - 2Nk_2x_3\right]_{\Sigma^*{}_1} \\ (f_3)_{\Sigma^*{}_1} = & \dfrac{L}{2\pi r}[-4\pi l_4 + k_1x_1 + k_2x_2]_{\Sigma^*{}_1} \end{cases} \tag{1.39}$$

$$\Sigma^*{}_2 \qquad \begin{cases} (f_1)_{\Sigma^*{}_2} = & \dfrac{1}{2\pi R}\left[-2Nh_2 - \left(\dfrac{N}{A}-1\right)(A+N\log\rho^2)k_3x_1 + 2Nk_1x_3\right]_{\Sigma^*{}_2} \\ (f_2)_{\Sigma^*{}_2} = & \dfrac{1}{2\pi R}\left[2Nh_1 - \left(\dfrac{N}{A}-1\right)(A+N\log\rho^2)k_3x_2 + 2Nk_2x_3\right]_{\Sigma^*{}_2} \\ (f_3)_{\Sigma^*{}_2} = & \dfrac{L}{2\pi R}[4\pi l_4 - k_1x_1 - k_2x_2]_{\Sigma^*{}_2} \end{cases} \tag{1.40}$$

$$\alpha^*{}_1 \qquad \begin{cases} (f_1)_{\alpha^*{}_1} = & \dfrac{L}{2\pi}\left[k_1 + \dfrac{1}{\rho^2}(h_3x_2 - 4\pi l_4x_1)\right]_{\alpha^*{}_1} \\ (f_2)_{\alpha^*{}_1} = & \dfrac{L}{2\pi}\left[k_2 - \dfrac{1}{\rho^2}(h_3x_1 + 4\pi l_4x_2)\right]_{\alpha^*{}_1} \\ (f_3)_{\alpha^*{}_1} = & -\dfrac{Fk_3}{2\pi}\left[1 + \left(1+\log\rho^2\right)\dfrac{N}{A}\right]_{\alpha^*{}_1} \end{cases} \tag{1.41}$$

$$\alpha^*{}_2 \qquad \begin{cases} (f_1)_{\alpha^*{}_2} = & \dfrac{L}{2\pi}\left[-k_1 - \dfrac{1}{\rho^2}\left(h_3x_2 - 4\pi l_4x_1\right)\right]_{\alpha^*{}_2} \\ (f_2)_{\alpha^*{}_2} = & \dfrac{L}{2\pi}\left[-k_2 + \dfrac{1}{\rho^2}\left(h_3x_1 + 4\pi l_4x_2\right)\right]_{\alpha^*{}_2} \\ (f_3)_{\alpha^*{}_2} = & \dfrac{Fk_3}{2\pi}\left[1 + \left(1+\log\rho^2\right)\dfrac{N}{A}\right]_{\alpha^*{}_2} \end{cases} \tag{1.42}$$

Conclusion If a hollow elastic cylinder, homogeneous and transversally isotropic $\mathcal{C}$, is initially found in a natural state $\mathcal{C}_\tau^*$ and experiences a many–valued isotermic displacement $\mathcal{C}_\tau^* \to \mathcal{C}_\tau$ as in (1.23), (and consequently a regular deformation), then, in the equilibrium configuration $\mathcal{C}_\tau$, a stress (1.38) and a congruent deformation (1.37) are present in every internal point; and surface forces (1.39)–(1.42) equivalent to zero are exerted on the boundary.

Remark While displacement (1.35) and tensor field of strain (1.37)) depend only on the ratio N/A, the tensor field of stress (1.38) depends on four of the five elastic constants.

Chapter 2

Analysis of distortions through Saint Venant's theory

This chapter deals with the analysis of the sixth elementary Volterra's distortion for a circular hollow, homogeneous, elastic, isotropic cylinder. More precisely, the specific load connected to the sixth distortion is proved to be equivalent (in Saint Venant's theory) to a right combined compressive and bending stress and to a right combined tensile and bending stress. These results have been applied to a material made up of steel to compare the obtained numerical results with Volterra's predictions: the values calculated through Saint Venant's theory are more strictly related to those calculated by Volterra when the cylinder thickness tends to zero [11].

2.1 Introduction

The first original and fundamental contribution to the dislocation theory was found in Weingarten's note [54] where it is shown that, in absence of external forces, equilibrium configurations for elastic bodies with non–zero internal stress can exist. Given, for example, an elastic ring initially in a natural configuration, one can create a state of deformation, and therefore of stress, by making a radial cut adding a thin slice of matter and finally soldering the two faces of the cut. The solid assumes a new equilibrium configuration (spontaneous equilibrium configuration); obviously, it isn't a natural equilibrium configuration since, adding matter, non–zero internal stress can be found.

Weingarten raised the problem and indicated some concrete examples with this anomalous behavior, but he didn't give analytic instruments to tackle and solve it. A fundamental contribution in this direction was given by Volterra, who used Weingarten's note as a starting point to develop a general theory. Volterra began with the observation that Weingarten's considerations could not be validated in case of simply–connected bodies in the range of regular deformations. Hence, Volterra proposed a new theory of elastic distortions [1] that implied a deep revision of the mathematical theory of elasticity in the case of multi–connected domains: when in analytic structure of solutions multivalued terms appear, theorems of uniqueness can't be valid in equilibrium problems with assigned forces [30, 52]. Note that in case of multi–connected domains, these terms, being physically admissible, can't be discarded (as one does, in order to have uniqueness of solution, in simply–connected domains where multivalued terms have no physical meaning); hence to obtain an uniqueness theorem isn't enough to assign external forces, but it is necessary to know the physically admissible multivalued properties.

The most general elastic distortion able to bring a right, circular, homogenous, hollow, isotropic cylinder to a state of spontaneous equilibrium, consists of six elementary distortions. For each, Volterra has tried to determine a field of displacements which fulfills the indefinite equations of elastic equilibrium and brings the body to a spontaneous equilibrium configuration. Really, Volterra was only able to determine a field of displacement that brings the cylinder to an equilibrium configuration, generating a distribution of forces globally equivalent to zero but not identically vanishing. So the problem of distortion was partially, but not totally solved. [2]

In the context of Volterra's partially results, this work analyzes the forces induced by the sixth elementary distortion on the right circular, homogenous, hollow, isotropic cylinder with a different point of view. More precisely, exploiting Saint Venant's theory and generalizing some previous results [9, 10], we have underlined that, apart from a limited zone in the

[1] The notion of distortion has been proposed by Volterra [51, 52] about one hundred years ago. The term has undergone some changes: in Love's book [42] the distortions were called dislocations. Presently, the word–combination "Volterra's distortions" is stable and identifiable: the term distortions is used for designations of phenomena creating the stress–strain state, when the external forces are absent (for example, the inhomogeneous temperature field can create the distortion) [18, 56].

[2] Since Volterra considered exclusively isotropic hollow cylinders, Caricato recently proposed an extension of the theory of Volterra's distortions to the case of a transversally isotropic homogeneous elastic hollow cylinder [17]; later on his findings have been reconsidered and expanded in [37]. Recently, the non linear aspect of distortion has been analyzed in [18, 56].

immediate vicinity of bases, the distribution of forces, considered as a specific load, can be replaced with one statically equivalent. This can be done without consequences on the effective distributions of stress and strain, and therefore, without the necessity to define the effective punctual distribution of this load acting on the bases of the cylinder.
Because of the homogeneity and isotropy of the material and of the geometric and loading symmetry of the body, we have approached the specific load as linear, constructed an auxiliary bar which has as longitudinal section the axial section of the cylinder and followed the basic considerations of Saint Venant's theory. We have found the specific load connected to the sixth distortion is equivalent (in Saint Venant's theory) to a right combined compressive and bending stress and to a right combined tensile and bending stress.

This chapter is organized as follows: in section 2 the general theory of Volterra's distortions is briefly recalled. In section 3 the specific load is analyzed by Saint Venant's theory. In section 4 numerical results and their comparison with Volterra's predictions are discussed.

2.2 Volterra's distortions for a circular hollow cylinder

Let's consider a circular hollow (therefore doubly connected) cylinder, which is, at a certain assigned temperature, in a natural state C. This we will assume as the reference configuration. This solid is depicted in Figure 1 with one cross section to which a generic point P belongs. We introduce into an ordinary space a Cartesian rectangular reference $0x_1x_2x_3$ with respective versors $\{\mathbf{c}_1, \mathbf{c}_2, \mathbf{c}_3\}$ and we choose the axis $0x_3$ coinciding with the symmetry axis of the cylinder and the coordinate plane $0x_1x_2$ placed over the base. We indicate with $\rho(\mathbf{x}) = \sqrt{\mathbf{x_1^2} + \mathbf{x_2^2}}$ and $\theta(\mathbf{x}) = arctg\frac{x_2}{x_1}$ respectively, the distance of P from the axis of the cylinder and the anomaly.

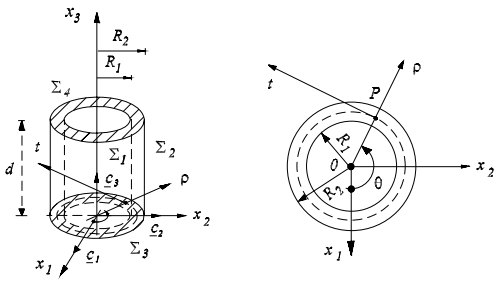

Figure 2.1: The hollow cylinder in the natural state and one of its cross sections

Hereafter, we call Σ the surface of C, made from the two cylindrical coaxial surfaces Σ_1 (internal surface of radius R_1) and Σ_2 (external surface of radius R_2), and from the two bases Σ_3 (at height $x_3 = 0$) and Σ_4 (at the height $x_3 = d$).

Let $\mathbf{u}(\mathbf{x})$ be the displacement vector which is the solution of the elastic equilibrium problem for a body subjected to given external forces (without external constraints and mass forces); let's assume that $\mathbf{u}(\mathbf{x})$ includes a multivalued term related to $\theta(\mathbf{x})$. This term is

physically significant in a doubly–connected region of space, as a body with hollow cylindrical symmetry.
The multivalued field of displacement $\mathbf{u}(\mathbf{x})$ has been physically interpreted by Volterra [52] in terms of the following operations:
if the doubly connected cylinder is transformed into one which is simply connected by a transversal cut on an axial semi–plane having the x_3 axis as edge, the vector $\mathbf{u}(\mathbf{x})$ can be characterized by a discontinuity of the first type through the semi-plane of the cut. If a translatory and a rotatory displacement is imposed on one of the faces of the cut by the application, at constant temperature, of a system of external forces, a state of deformation, and therefore of stress due to the multivalued term including $\theta(\mathbf{x})$, is created into the cylinder. In order that the cylinder remains in a state of *spontaneous equilibrium* in the deformed configuration, i.e. with a regular internal stress but absent of superficial forces, it is enough to re-establish the continuity remaking the cylinder doubly connected by soldering the two faces of the cut (they are soldered by adding or removing a thin slice of matter). In this way a distortion in the multi–connected body is induced.
In addition, since the rigid displacement of a face of cut with respect to the other can be obtained through a rigid translation displacement and a rigid rotation displacement, a distortion can be described by six constant parameters l, m, n, p, q, r, called *characteristic coefficients of distortion*. They correspond to the three Cartesian components of translation and rigid rotation in respect to the axes x_1, x_2, x_3. Once the characteristic coefficients are introduced, we can give the following:

Definition 1. *Elementary distortion is the definition of the distortion that has only one of the six characteristic coefficients different from zero [30, 47, 52]. Analogously, the displacement induced by an elementary distortion has non–zero only one of the following coefficients* l, m, n, p, q, r.

So making, Volterra characterized six independent distortions that are showed in the following Figure 2: In particular, the 6^{th} elementary distortion is the distortion related to the

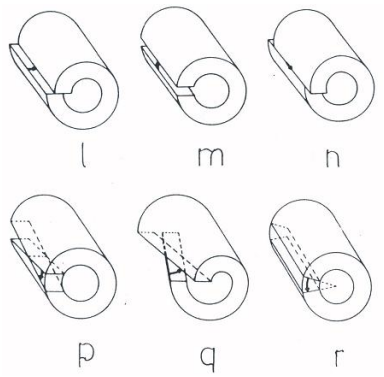

Figure 2.2: The six elementary Volterra's distortions.

coefficient r. It is realized by cutting the cylinder with an axial plane, rotating the face of

the cut that faces the semi–plane $x_2 < 0$ and, after adding (when $r > 0$) or removing (when $r < 0$) a thin slide of matter, soldering the sides.
Note that the axial plane of the cut can be, for example, the plane $0x_1x_3$. However, since the elementary distortion is uniquely characterized by the value of r (and not by the particular plane having the axis Ox_3 as edge), it is not essential that the plane chosen to determine the 6^{th} elementary distortion corresponds to the coordinate plane Ox_1x_3.

2.2.1 Forces on the bases: Volterra's analysis

Volterra, after having analyzed the elastic distortion from a qualitative point of view, has partially dealt and solved the problem from a purely mathematics point of view [52]. In particular, he focused his attention on a linearly elastic, isotropic, homogeneous, doubly–connected cylinder with finite height d. The study of doubly–connected body only it is not restrictive since the analysis of multi–connected bodies requires more complex analytic problems and hence, more complex computation, but it adds nothing of conceptual interest [52].
Now, in order to briefly recall Volterra's considerations for the sixth elementary distortion, let's refer to cylindric coordinates and call (P, ρ^*, t^*, x_3^*) the counterclockwise rectangular reference system obtained by translating in P the axes ρ, t and x_3 (see Figure 3)

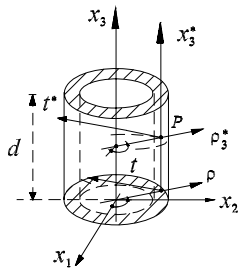

Figure 2.3: Hollow cylinder referred to cartesian and cylindrical reference system

More precisely, for forces acting only on the bases, the components of a displacement vector $\mathbf{u}(P)$ related to the 6^{th} elementary distortions are [42, 43, 47, 49, 52]:

$$\begin{cases} u_{\rho^*}(\rho,\theta,x_3) = -\dfrac{r}{2\pi}\,\rho\left[\dfrac{1}{2} - \dfrac{\mu}{2(\lambda+2\mu)}\left(\log\rho^2 - \dfrac{R_2^2\log R_2^2 - R_1^2\log R_1^2}{R_2^2 - R_1^2}\right) + \right. \\ \qquad\qquad \left. + \dfrac{1}{\rho^2}\dfrac{\lambda+\mu}{\lambda+2\mu}\,R_1^2R_2^2\,\dfrac{\log R_2^2 - \log R_1^2}{R_2^2 - R_1^2}\right] \\ u_{t^*}(\rho,\theta,x_3) = \dfrac{r}{2\pi}\,\rho\,\theta \\ u_{x_3^*}(\rho,\theta,x_3) = 0 \end{cases} \tag{2.1}$$

where μ and λ are the two Lamé constants.
$\mathbf{u}(P)$ satisfies the indefinite equations of elastic equilibrium in the absence of forces of mass

and generates a distribution of surface forces on the bases $\sum_3$ and $\sum_4$. In (O, ρ, θ, x_3), this distribution has the following independent from θ coomponents (see [42, 47, 52]):

$$\begin{cases} f_\rho(\rho, 0) = 0 \\ f_t(\rho, 0) = 0 \\ f_{x_3}(\rho, 0) = \dfrac{r}{2\pi} \dfrac{\lambda\mu}{\lambda + 2\mu} \left(1 + \log \rho^2 - \dfrac{R_2^2 \log R_2^2 - R_1^2 \log R_1^2}{R_2^2 - R_1^2} \right) = -a[b + \log \rho^2] \ ; \end{cases}$$

$$\begin{cases} f_\rho(\rho, d) = 0 \\ f_t(\rho, d) = 0 \\ f_{x_3}(\rho, d) = -\dfrac{r}{2\pi} \dfrac{\lambda\mu}{\lambda + 2\mu} \left(1 + \log \rho^2 - \dfrac{R_2^2 \log R_2^2 - R_1^2 \log R_1^2}{R_2^2 - R_1^2} \right) = a[b + \log \rho^2] \end{cases} \tag{2.2}$$

where

$$a = -\frac{r}{2\pi} \frac{\lambda\mu}{\lambda + 2\mu}$$

and

$$b = 1 - \frac{R_2^2 \log R_2^2 - R_1^2 \log R_1^2}{R_2^2 - R_1^2}.$$

2.3 Analysis of the specific load as characteristic of the external solicitation

In this section we will analyze the solution of the elastic equilibrium proposed by Saint Venant for a prismatic isotropic homogeneous linearly elastic solid subjected to a specific load on the bases.

In Saint Venant's theory one can replace the specific load with an equivalent one. In this way, apart from a thin zone near the bases, called *extinction zone*, we have no consequences on the effective distribution of stress and strain. So, every solution of the problem of the elastic equilibrium can be considered as a solution of an infinity of cases which are pertinent to an infinity of load models, distributed with different laws, but having the same resultant. This resultant can be replaced, as we know from static, by a force through a generic point P' belonging to the base section, and by a couple that has, in respect to P', the same moment of the resultant. Note that the resultant is applied in a suitable point, generally different from P'.

Since the force and the couple can be decomposed with respect to the three axes of the reference system, the six *characteristics of the external solicitation*, i.e. the three components of the force and of the couple, are individuated.

Hence, since these characteristics completely define every system of external loads acting on the bases of the solid, it is unnecessary to define their effective punctual distributions. As a consequence, the more general case can be solved through a linear combination of six elementary cases: normal stress, shear stress along x_2, shear stress along x_1, bending moment around x_1, bending moment around x_2 and torsional moment.

2.3.1 Saint Venant's theory to analyze the sixth elementary distortion

This section deals with the analysis the specific load in Saint Venant's theory (see [9, 31, 10]). Hereafter, we will assume that the hollow cylinder is thin (i.e. its thickness $\Delta\rho = R_2 - R_1$ is small with respect to the radius R_1) and we will consider just the vertical component of the load, i.e. $f_{x_3}(\rho, d)$, acting on the base $x_3 = d$. It is clear that, for the equilibrium, the vertical component acting on the inferior base $x_3 = 0$, will be directly opposed.
$f_{x_3}(\rho, d)$ can be simply denoted with $f(\rho)$, since, once x_3 is fixed, it is a function of ρ only.

Moreover, since $f(\rho)$ is monotone in $[R_1, R_2]$, the equation $f(\rho) = 0$ has in (R_1, R_2) one real root:

$$\rho_n = \sqrt{e^{\dfrac{R_2^2 \log R_2^2 - R_1^2 \log R_1^2}{R_2^2 - R_1^2} - 1}} \ . \tag{2.3}$$

In other words, ρ_n is the value or the radius of the cylindrical neutral surface of the hollow body with respect to the specific load.
Note that in every axial section, since the deformed hollow cylinder has stretched and compressed bending fibres to conserve its original volume, $R_1 < \rho_n < R_2$ must be verified. In addition (see [52, p. 435] and Figure 4)

$$\rho_M < \rho_n < R_2 \ , \tag{2.4}$$

where

$$R_M \ = \ \rho_M = \frac{R_1 + R_2}{2} \ .$$

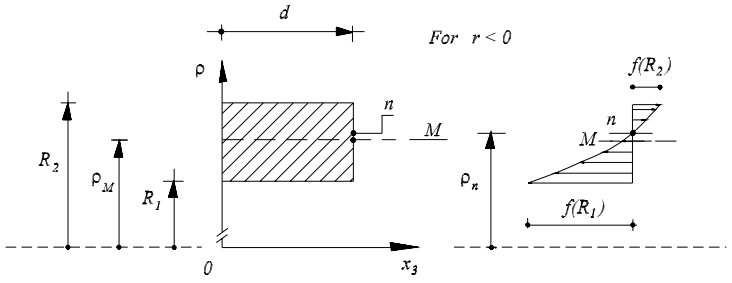

Figure 2.4: Specific load distribution

Now, let's consider a simply connected auxiliary rectangular beam. We suppose that it has height d (i.e. the same height of the cylinder) and cross section with unitary base for convenience. More precisely, we suppose that the cross section of the auxiliary beam is a rectangle whose area is $(R_2 - R_1) * 1$ and if we consider an axial section of the cylinder of height d, then it can be assimilated to a longitudinal section of the auxiliary beam.
Moreover, the auxiliary beam is subjected to the load $f(\rho)$ on the bases.

With reference to the aforementioned beam, from Eq. (2.4) we obtain that, in modulus, the area delimited by $f(\rho)$ on $[R_1, \rho_n]$ is greater than that delimited on $[\rho_n, R_2]$:

$$\left| \int_{R_1}^{\rho_n} f(\rho) d\rho \right| > \left| \int_{\rho_n}^{R_2} f(\rho) d\rho \right| \ .$$

Now we would like to analyze the two zones delimitated by ρ_n (see Figure 4) and separately study the distribution of load.
More precisely, since in Saint Venant's theory it is unnecessary to define the effective punctual distribution of the load on the bases of the body, we will appropriately reduce the load induced in each section by the sixth elementary distortion to a normal stress and to a couple.
The normal stress and the momentum of the couple, both applied in the barycenter of the section, will have a fundamental role in our analysis; more precisely, they allow us to prove the specific load connected to the sixth distortion is equivalent (in Saint Venant's theory) to a right combined compressive and bending stress and to a right combined tensile and bending stress. These ideas will be developed in detail in the following sections.

Upper section: $\rho \in [\rho_n, R_2]$

Let's focus our attention on $\rho \in [\rho_n, R_2]$; let ρ_e be the value of ρ where we have to translate the diagram of $f(\rho)$ to divide the upper section in two with, in modulus, the same area (see Figure 5).
The explicit value of ρ_e is obtained by solving the following equation:

$$\int_{\rho_n}^{\rho_e} [f(\rho) - f(\rho_e)] \, d\rho + \int_{\rho_e}^{R_2} [f(\rho) - f(\rho_e)] \, d\rho = 0 \ ;$$

from which we easily derive

$$\rho_e = \sqrt{e^{-\frac{2R_2 - 2\rho_n - R_2 \log R_2^2 + \rho_n \log \rho_n^2}{R_2 - \rho_n}}} \ .$$

As already underlined, the specific load acting on the section can be represented by a normal stress $\mathbf{N}$ applied on the barycenter G_1 of the section whose modulus is

$$N \ = \ f(\rho_e)(R_2 - \rho_n) = a(R_2 - \rho_n)(b + \log \rho_e^2) \ ,$$

and by a couple $(\mathbf{C}_1, -\mathbf{C}_1)$, whose vectors are applied in $G_1^{(1)}$ and $G_1^{(2)}$ respectively, i.e. in the barycenters of the two sections having the same area (see Figure 5).
So, in order to evaluate the couple, its arm and the coordinate of its center, we want to specify the positions of these barycenters.

More precisely, using the technique of static momenta, we compute the values of ρ corresponding to the two barycenters; so, by the formula

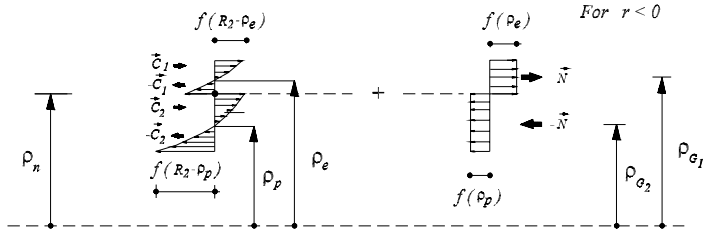

Figure 2.5: Decomposition of the specific load

$$\rho_{G_1^{(1)}} = \frac{\displaystyle\int_{\rho_e}^{R_2} \rho\,[f(\rho) - f(\rho_e)]\,d\rho}{\displaystyle\int_{\rho_e}^{R_2} [f(\rho) - f(\rho_e)]\,d\rho}\ ,$$

we have

$$\rho_{G_1^{(1)}} = \frac{R_2^2 - \rho_e^2 - 2R_2^2(\log R_2 - \log \rho_e)}{4[R_2 - \rho_e - R_2(\log R_2 - \log \rho_e)]}\ ;$$

while

$$\rho_{G_1^{(2)}} = \frac{\rho_e^2 - \rho_n^2 - 2\rho_n^2(\log \rho_e - \log \rho_n)}{4[\rho_e - \rho_n - \rho_n(\log \rho_e - \log \rho_n)]}\ ,$$

obtained by the analogous formula

$$\rho_{G_1^{(2)}} = \frac{\displaystyle\int_{\rho_n}^{\rho_e} \rho\,[f\ (\rho) - f(\rho_e)]\,d\rho}{\displaystyle\int_{\rho_n}^{\rho_e} [f(\rho) - f(\rho_e)]\,d\rho}\ .$$

Moreover, referring to the area

$$\int_{\rho_e}^{R_2} [f(\rho) - f\ (\rho_e)]\,d\rho\ ,$$

it is possible to evaluate the modulus of the vector $\mathbf{C}_1$

$$C_1\ =\ a\left[2(R_2 - \rho_e) - R_2(\log R_2^2 - \log \rho_e^2)\right]\ .$$

It is clear that, referring to the area $\displaystyle\int_{\rho_n}^{\rho_e} [f(\rho) - f\ (\rho_e)]\,d\rho$, when we evaluate the modulus of the second vector of the couple it is is equal to $a\left[2\rho_e - 2\rho_n - \rho_n(\log \rho_e^2 - \log \rho_n^2)\right]$. Note that

since the evaluated areas are equal, this vector can be called $-\mathbf{C}_1$.
As the vectors of the couple are applied in the barycenter of the two equivalent sections, its arm is $b_1 = (\rho_{G_1^{(1)}} - \rho_{G_1^{(2)}})$, the coordinate of its center D_1 is $\rho_{D_1} = \frac{\rho_{G_1^{(1)}} + \rho_{G_1^{(2)}}}{2}$, and its momentum $\mathbf{M}_{D_1}$ has, in modulus, the following expression:

$$M_{D_1} = b_1\, C_1 = a(\rho_{G_1^{(1)}} - \rho_{G_1^{(2)}}) \left[2R_2 - 2\rho_e - R_2(\log R_2^2 - \log \rho_e^2)\right] .$$

In order to obtain the load globally acting on the section (normal stress and momentum of the couple both applied in the same point, i.e. in D_1), we need to translate $\mathbf{N}$ in D_1 and hence evaluate, in modulus, the momentum $\mathbf{M}'_{D_1}$ related to this translation:

$$\begin{aligned} M'_{D_1} &= (\rho_{G_1} - \rho_{D_1})\, f(\rho_e)(R_2 - \rho_n) = \\ &= a[b + \log \rho_e^2](R_2 - \rho_n) \left[\frac{R_2 + \rho_n}{2} - \frac{(\rho_{G_1^{(1)}} + \rho_{G_1^{(2)}})}{2}\right] . \end{aligned}$$

So, the total momentum applied in D_1 is

$$\begin{aligned} M''_{D_1} &= M'_{D_1} + M_{D_1} = \\ &= \frac{1}{2} a(R_2 - \rho_n)(\rho_n - \rho_{G_1^{(1)}} - \rho_{G_1^{(2)}} + R_2)(b + \log \rho_e^2) + \\ &\quad -a(\rho_{G_1^{(1)}} - \rho_{G_1^{(2)}})[2R_2 - 2\rho_e - R_2(\log R_2^2 - \log \rho_e^2)] . \end{aligned}$$

Note that the center D_1 doesn't coincide with the barycenter of the section:

$$\rho_{D_1} < \rho_{G_1} = \frac{R_2 + \rho_n}{2} .$$

Because of this limitation and the sign of $\mathbf{N}$, then $\mathbf{M}'_{D_1}$ and $\mathbf{M}_{D_1}$ have opposite signs. Moreover, M''_{D_1} is less then M_{D_1}, but has its sign.

Once the explicit form of M''_{D_1} is known, we can compute the eccentricity $e_{C_{S,1}}$ of the normal stress $\mathbf{N}$ with respect to the point D_1 (see Figure 6), and hence, the position of the center of stress $C_{S,1}$. Note that $C_{S,1}$ characterizes the point belonging to the meridian plane (that is also plane of stress) where one can apply only the normal stress to obtain the same effect produced by the specific load acting on the bases of the cross section of the auxiliary beam. More precisely, in the coordinate–plane $(0, \rho, x_3)$,

$$\rho_{C_{S,1}} = e_{C_{S,1}} + \rho_{D_1} = \frac{M''_{D_1}}{N} + \frac{1}{2}(\rho_{G_1^{(1)}} + \rho_{G_1^{(2)}}) .$$

Finally, since Saint Venant's theory refers to the barycenter, we have to evaluate the momentum $\mathbf{M}_{G_1}$ of $\mathbf{N}$ with respect to G_1. So, letting

$$b'_1 = \rho_{C_{S,1}} - \rho_{G_1} = -\frac{(\rho_{G_1^{(1)}} - \rho_{G_1^{(2)}}) \left[2R_2 - 2\rho_e - R_2 \left(\log R_2^2 - \log \rho_e^2\right)\right]}{(R_2 - \rho_n)\,(b + \log \rho_e^2)}$$

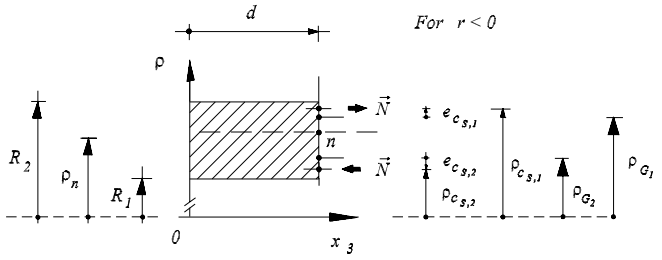

Figure 2.6: Centers of stress and their positions

be the arm, we have

$$M_{G_1} \;=\; b_1' N = -a\left(\rho_{G_1^{(1)}} - \rho_{G_1^{(2)}}\right)\left[2R_2 - 2\rho_e - R_2\left(\log R_2^2 - \log \rho_e^2\right)\right] .$$

Then, in agreement with Saint Venant's theory, for all $z \in [0, d]$ in the section there is the action of the following linear $\sigma_{x_3}^{(1)}(\rho)$ (right combined tensile and bending stress):

$$\sigma_{x_3}^{(1)}(\rho) = \frac{N}{L_1} + \frac{M_{G_1}}{I_{G_1}}\left(\rho - \frac{R_2+\rho_n}{2}\right) =$$

$$= f(\rho_e) + \\ - \frac{12a(\rho_{G_1^{(1)}} - \rho_{G_1^{(2)}})\left[2R_2 - 2\rho_e - R_2\left(\log R_2^2 - \log \rho_e^2\right)\right]}{(R_2-\rho_n)^3}\left(\rho - \frac{R_2+\rho_n}{2}\right) =$$

$$= a(b + \log \rho_e^2) + \\ - \frac{12a(\rho_{G_1^{(1)}} - \rho_{G_1^{(2)}})\left[2R_2 - 2\rho_e - R_2\left(\log R_2^2 - \log \rho_e^2\right)\right]}{(R_2-\rho_n)^3}\left(\rho - \frac{R_2+\rho_n}{2}\right) . \qquad (2.5)$$

Actually, L_1 is reduced to $R_2 - \rho_n$ since the cross section of the bar has unitary bases; moreover, $I_{G_1} = \frac{1}{12}(R_2 - \rho_n)^3$, as it is known, is the momentum of inertia in respect to an axis through G_1 and parallel to the bases of the same cross section.

Lower section: $\rho \in [R_1, \rho_n]$

Let's consider the lower section where $\rho \in [R_1, \rho_n]$. In order to obtain, in Saint Venant's theory, the explicit form of the stress acting on the bases of the auxiliary beam, we briefly recall the same strategy amply described in the previous case. So

$$\rho_p = \sqrt{e^{-\frac{2\rho_n - 2R_1 - \rho_n \log \rho_n^2 + R_1 \log R_1^2}{\rho_n - R_1}}}$$

is the point where we have to translate the diagram of $f(\rho)$ to obtain the division of the lower section into two smaller ones with, in modulus, the same area. The normal stress applied to

the barycenter G_2 of the section, whose $\rho_{G_2} = \frac{\rho_n + R_1}{2}$, is in modulus

$$N \;=\; f(\rho_p)(\rho_n - R_1) \;=\; a(\rho_n - R_1)(b + log\rho_p^2)\ .$$

Moreover, we can evaluate the couple $(\mathbf{C}_2, -\mathbf{C}_2)$

$$C_2 \;=\; a\left[2(\rho_n - \rho_p) - \rho_n(\log\rho_n^2 - \log\rho_p^2)\right]\ ,$$

its arm

$$b_2 \;=\; \rho_{G_2^{(1)}} - \rho_{G_2^{(2)}} \;=$$

$$= \frac{\rho_n^2 - \rho_p^2 - 2\rho_n^2(\log\rho_n - \log\rho_p)}{4[\rho_n - \rho_p - \rho_n(\log\rho_n - \log\rho_p)]} - \frac{\rho_p^2 - R_1^2 - 2R_1^2(\log\rho_p - \log R_1)}{4[\rho_p - R_1 - R_1(\log\rho_p - \log R_1)]}\ ,$$

and clearly the coordinate of its center D_2

$$\rho_{D_2} \;=\; \frac{\rho_{G_2^{(1)}} + \rho_{G_2^{(2)}}}{2}\ .$$

Following the same line of reasoning, we can consider

$$\begin{aligned} M''_{D_2} \;\;&=\;\; = \frac{1}{2}a(\rho_n - R_1)(\rho_n - \rho_{G_2^{(2)}} - \rho_{G_2^{(1)}} + R_1)(b + \log\rho_p^2) + \\ &\quad -a(\rho_{G_2^{(1)}} - \rho_{G_2^{(2)}})[2\rho_n - 2\rho_p - \rho_n(\log\rho_n^2 - \log\rho_p^2)]\ , \end{aligned}$$

and hence

$$\rho_{C_{S,2}} \;=\; e_{C_{S,2}} \;+\; \rho_{D_2} \;=\; \frac{M''_{D_2}}{N} + \frac{1}{2}(\rho_{G_2^{(1)}} + \rho_{G_2^{(2)}})\ .$$

Finally, since Saint Venant's theory refers to the barycenter, we have to evaluate the momentum $\mathbf{M}_{G_2}$ of $\mathbf{N}$ with respect to G_2. So, letting

$$b'_2 = -\frac{(\rho_{G_2^{(1)}} - \rho_{G_2^{(2)}})\left[2\rho_n - 2\rho_p - \rho_n\left(\log\,\rho_n^2 - \log\,\rho_p^2\right)\right]}{(\rho_n - R_1)\left(b + \log\,\rho_p^2\right)}$$

be the arm, we have

$$M_{G_2} = -a\left(\rho_{G_2^{(1)}} - \rho_{G_2^{(2)}}\right)\left[2\rho_n - 2\rho_p - \rho_n\left(\log\,\rho_n^2 - \log\,\rho_p^2\right)\right]\ .$$

Thus, in agreement with Saint Venant's theory, for all $z \in [0, d]$ in the section there is the action of the following linear $\sigma_{x_3}^{(2)}(\rho)$ (right combined compressive and bending stress):

$$\sigma_{x_3}^{(2)}(\rho) = \frac{N}{L_2} + \frac{M_{G_2}}{I_{G_2}}\left(\rho - \frac{R_1 + \rho_n}{2}\right) =$$

$$\begin{aligned} &= a(b + \log\,\rho_p^2) + \\ &\quad - \frac{12a(\rho_{G_2^{(1)}} - \rho_{G_2^{(2)}})\left[2\rho_n - 2\rho_p - \rho_n\left(\log\,\rho_n^2 - \log\,\rho_p^2\right)\right]}{(\rho_n - R_1)^3}\left(\rho - \frac{R_1 + \rho_n}{2}\right). \end{aligned} \tag{2.6}$$

Actually, L_2 is reduced to $\rho_n - R_1$ since the cross section of the bar has unitary bases; moreover, $I_{G_2} = \frac{1}{12}(\rho_n - R_1)^3$, as it is known, is the momentum of inertia in respect to an axis through G_2 and parallel to the bases of the same cross section.

2.4 Numerical Results

The importance of Saint Venant's theory applied to the sixth elementary distortions is mainly based on the information content of the Eq. (2.5) and (2.6). More precisely, they underline what kind of load is induced (in Saint Venant's theory) by the sixth elementary distortion: it is a right combined tensile and bending stress and a right combined compressive and bending stress. Hence, for every axial section it is possible to evaluate the tensional state with the well–known Saint Venant's formulas [31].
However, in order to apply Saint Venant's theory, our analysis has required some assumptions: we have considered a suitable auxiliary beam and we have assumed that the load on the bases has a linear diagram. So, to evaluate the deviation of our results from Volterra's predictions, in this section we compare Eq. (2.5) and (2.6) with $f_{x_3}(\rho)$ computed by Volterra.

More precisely, let's consider the cylinder made of steel, for which

$$\lambda = 1.53 * 10^{-6} kg/cm^2 \; ; \; \nu = 7.89 * 10^5 kg/cm^2 \; ,$$

and let's subject the side of the cut to this rotation $r = -1.62 * 10^{-5}\ rad$.
The smallness of the chosen angle is justified by the required thickness of the cylinder, by the material it is made of and by the hypothesis that Saint Venant's theory is valid for small displacements.
Moreover, we fixed $R_2 = 4$ cm and then we examined the following two cases:

$$\beta = \frac{R_1}{R_2} = 0.5 \; ; \; \beta = \frac{R_1}{R_2} = 0.9$$

from which

$$R_1 = 2\,\mathrm{cm}\,, \Delta \mathrm{R} = 2\,\mathrm{cm} \; ; \; \mathrm{R}_1 = 3.6\,\mathrm{cm}\,, \Delta \mathrm{R} = 0.4\,\mathrm{cm} \; .$$

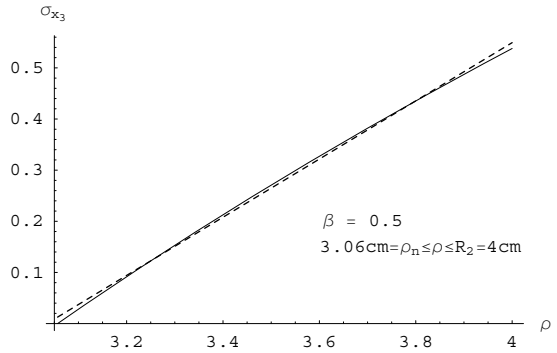

Figure 2.7: Load in Volterra 's theory (black) and load in our results (dashed) for $\beta = 0.5$. The picture refers to the upper section, i.e. $3.06\,\mathrm{cm} = \rho_n \leq \rho \leq R_2 = 4$ cm

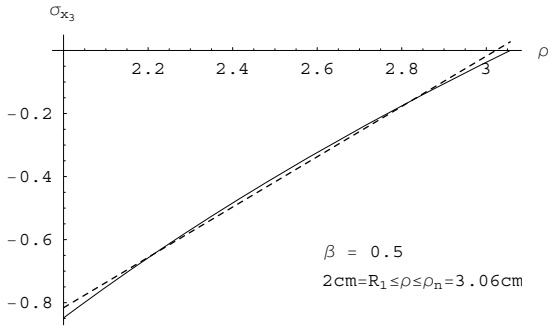

Figure 2.8: Load in Volterra 's theory (black) and load in our results (dashed) for $\beta = 0.5$. The picture refers to the lower section, i.e. $2\,\text{cm} = R_1 \leq \rho \leq \rho_n = 3.06$ cm

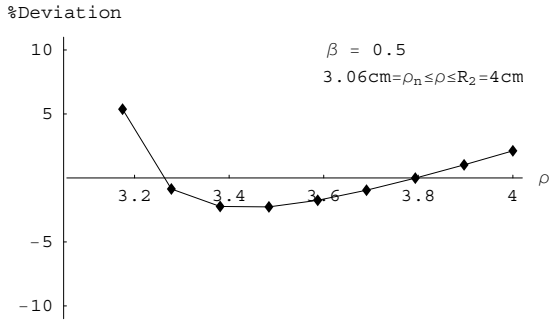

Figure 2.9: Graphic representation of the percent deviation of our results from Volterra's prediction for $\beta = 0.5$ and $3.06\,\text{cm} = \rho_n \leq \rho \leq R_2 = 4$ cm

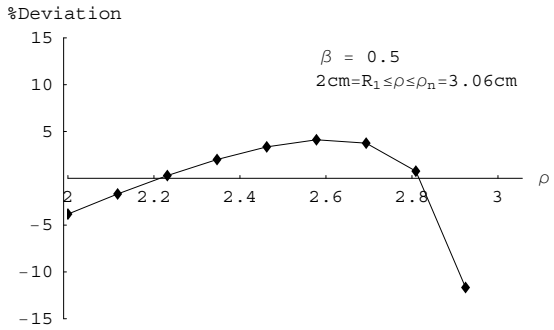

Figure 2.10: Graphic representation of the percent deviation of our results from Volterra's prediction for $\beta = 0.5$ and $2\,\text{cm} = R_1 \leq \rho \leq \rho_n = 3.06$ cm

When $\beta = 0.5$, in Figure 7 and Figure 8 we have shown the graphics of the different loads. These pictures clearly demonstrate that the dashed line (expression of load in our results) is a good approximation of Volterra's prediction. The percent deviation of our result

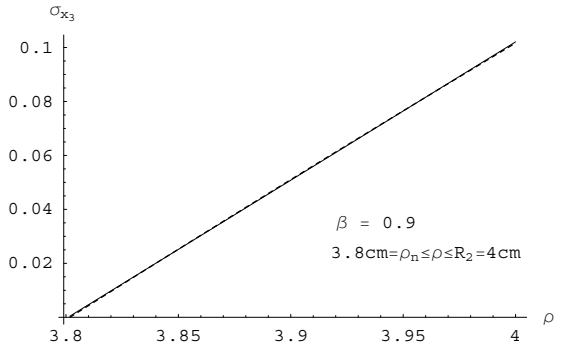

Figure 2.11: Load in Volterra 's theory (black) and load in our results (dashed) for $\beta = 0.9$. The picture refers to the upper section, i.e. $3.8\,\text{cm} = \rho_n \le \rho \le R_2 = 4$ cm. Note that the two lines are indistinguishable

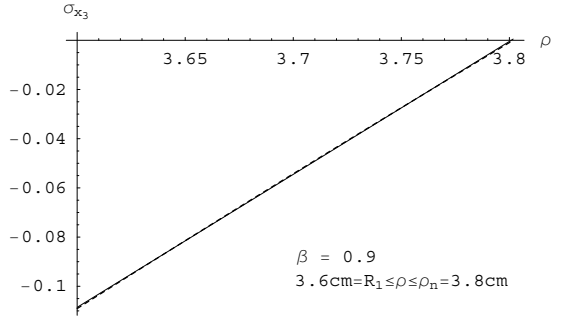

Figure 2.12: Load in Volterra 's theory (black) and load in our results (dashed) for $\beta = 0.9$. The picture refers to the lower section, i.e. $3.6\,\text{cm} = R_1 \le \rho \le \rho_n = 3.8$ cm. Note that the two lines are indistinguishable

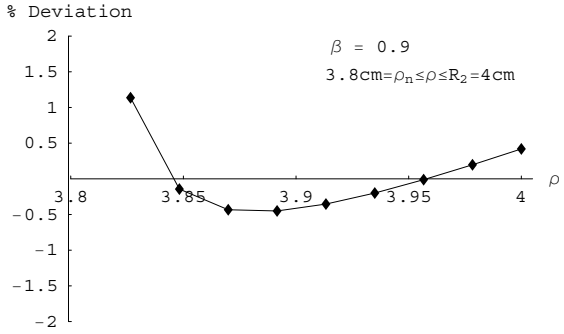

Figure 2.13: Graphic representation of the percent deviation of our results from Volterra's prediction for $\beta = 0.9$ and $3.8\,\text{cm} = \rho_n \le \rho \le R_2 = 4$ cm

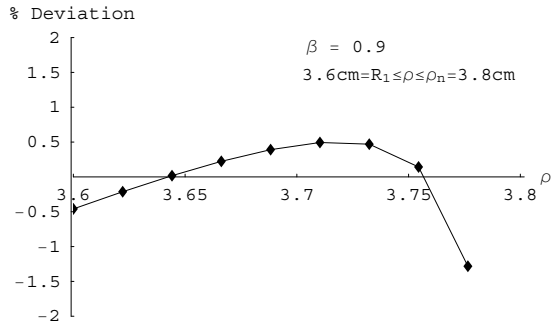

Figure 2.14: Graphic representation of the percent deviation of our results from Volterra's prediction for $\beta = 0.9$ and $3.6\,\text{cm} = R_1 \leq \rho \leq \rho_n = 3.8$ cm

from Volterra's formula, for different values of ρ, is shown in Figure 9 and Figure 10. This deviation is calculated dividing the difference between the load in Volterra's theory and the load in our results by the load in Volterra's theory. As already underlined in the analytic treatment of the previous section, apart from a small zone near the neutral axis this deviation is "small": the "error" made in such approximation can be strongly controlled.
Note that it is not restrictive to consider a small set of fixed ρ as to compute this deviation. In fact, apart from a small zone near the neutral axis, which thickness, in both cases, doesn't exceed the 16% of the thickness of the considered section, this deviation remains bounded by the same small value. Analyzing Figure 9 and Figure 10, it seems that this value is about 5. We want to underline that since $f_{x_3}(\rho)$ tends to zero in this small zone near the neutral axis, the aforementioned formula is unable to give us information on the percent deviation, that by Figure 7 and Figure 8 is bounded.

Finally, we have compared the obtained numerical results with Volterra's prediction for a very thin cylinder. More precisely, when $\beta = 0.9$, i.e. when that R_1 differs little from R_2, in Figure 11 and Figure 12 we have shown the graphics of the different loads. In this case it is rather impossible to distinguish between them. Clearly (see Figure 13 and Figure 14), apart from a small zone near the neutral axis, which thickness, in both cases, doesn't exceed the 16% of the thickness of the considered section, the deviation is also strongly bounded (about by 0.6 per cent).
We can conclude by seeing that the values calculated through Saint Venant's theory are more strictly related to those calculated by Volterra when the cylinder thickness tends to zero.

2.5 Conclusions

In this chapter we have improved Volterra's analysis focusing our attention on the load induced on the bases by one of the six elementary distortions, the sixth one. Precisely, taking advantage from the Saint Venant theory, tackled for our case, we have evaluated the nature of this force. In particular, approaching the specific load as linear one and constructing an auxiliary bar which has as longitudinal section the axial section of the cylinder, we have

analyzed the tensional state with the well known Saint Venant's principle.
We have obtained the specific load connected to the sixth distortion is equivalent (in Saint Venant's theory) to a right combined compressive and bending stress and to a right combined tensile and bending stress.
As previously underlined, this result is achieved by considering some assumptions and approximations. So, to evaluate its reliability and precision, we have added numerical simulations able to visualize, and hence compare, the load given by Volterra and the load computed through the Saint Venant's theory. The numerical analysis, applied to a thin steel cylinder, demonstrates that we have obtained a good approximations of Volterra's prediction: in all the analyzed cases, apart from the *extinction zone*, the deviation between the two expression of the same load remains strongly bounded. This gives reason to a possible generalization of the statement. More precisely, we stress that the various results obtained here are limited to the analysis of the sixth elementary distortion. As an interesting research perspective, we aim to address the generalization of our analysis to the case of a general distortion and which we are planning for forthcoming investigations.

Chapter 3

Mathematical model for para–ferromagnetic phase transitions

In this chapter, by an extension of the Ginzburg–Landau theory, it is proposed a mathematical model describing hard magnets within which we are able to explore the para–ferromagnetic transition and by using the Landau–Lifshitz–Gilbert equation, to study the 3D evolution of magnetic field. Finally, the hysteresis loops are obtained and represented by numerical implementations. Precisely, by an extension of the Ginzburg–Landau theory, it is proposed a mathematical model describing hard magnets within which we are able to explore the para–ferromagnetic transition and by using the Landau–Lifshitz–Gilbert equation, to study the 3D evolution of magnetic field. Finally, the hysteresis loops are obtained and represented by numerical implementations [24].

3.1 Introduction

Ferromagnetism is a typical phenomenon occurring in materials such as iron, cobalt, nickel and many alloys containing these elements. The ferromagnetic phase appears when a small external magnetic field yields a large magnetization inside the material, due to the alignment of the spin magnetic moments. Moreover, we observe a residual magnetization; namely, the spin magnetic moments stay aligned even if the external magnetic field vanishes.

It is well–known that ferromagnetic materials are characterized by a critical temperature θ_c, called the Curie temperature [1], [28], [35], [32]. For temperatures greater than θ_c, we have a paramagnetic behaviour. When the temperature crosses θ_c, the material undergoes a second order transition and displays ferromagnetic behaviour. In ferromagnetic materials we observe an easy magnetization, motivated by the property of atom patterns to displays a magnetic moment. In this work we propose a model for describing the para-ferromagnetic phase transition and for predicting the classical hysteresis loops bellow the critical temperature θ_c. The large magnetic field is due to the alignment patterns of their constituent atoms, which act as elementary electromagnets.

By an order parameter or phase field we mean a macroscopic variable describing the internal physical state of the material, given by some macroscopic (chemical and physical) properties. In the para–ferromagnetic transition we observe a different behaviour of the order parameter, which characterizes the nature of the transition [14], [28].

According to the modern classification due to Landau, phase transitions can be separated into two classes: first and second order transitions. In first order transitions, as long as θ does not cross θ_c, the phase field is a constant function in both the phases. This does not happen in second order transitions, in which the order parameter is constant in one of two phases only. In other papers, on all paramagnetic and ferromagnetic phases, the order parameter is not a constant, but a function of the magnetic field. In this work, in agreement with the definition of a second order phase transition, we propose a model such that in the paramagnetic phase the order parameter is a new variable, independent from magnetic field. Finally, within this range, we obtain the peculiar hysteresis loops characteristic of a hard magnet.

The present chapter is laid out as follows. In Secs. 2 and 3, we propose a model for studying the paramagnetic–ferromagnetic transition for a hard magnet, within which we also describe the ferromagnetic behaviour and the hysteresis loops due to change of phase field, magnetic effects and temperature.

In Sec. 4, we study the consistency of our model with thermodynamic laws. In agreement with this point of view, the first law of thermodynamics yields the heat equation related to our model.

Finally, in Sec. 5 and 6, for a unidimensional problem, we provides some numerical implementations of the model. Moreover, we study the magnetization induced by the magnetic field $\mathbf{H}$, described by a curve obtained by plotting the magnetic induction field $\mathbf{B}$ against the magnetic field $\mathbf{H}$. This curve shows the characteristic shape of a hysteresis loop. Finally, we demonstrate that the model ably describes the para–ferromagnetic phase transition, when the temperature θ crosses the Curie temperature θ_c.

3.2 Mathematical model

Ferromagnetism is usually studied by means of a macroscopic theory according to which inside a ferromagnet there are regions of microscopic dimensions, called Weiss domains, containing magnetic dipoles [55], [50], [45]. When no magnetic field is applied, the domains are oriented in order that the average magnetic field is zero. However, if an external magnetic field is applied, the boundaries of the domains move with the consequence that the regions, with spins parallel to the field, grow at the expense of the ones oriented in a different direction. The net effect is an internal distribution of the spins aligned with the field, leading to large value of the resulting magnetic field. If the external magnetic field is strong enough, all the magnetic dipoles are oriented with the magnetic field and the material is saturated, with the magnetic induction field $\mathbf{B}_s$. Even when the applied magnetic field is removed, the ferromagnet retains a residual magnetic induction $\mathbf{B}_r$. To reduce $\mathbf{B}_r$ to zero, one needs to apply a magnetic field $-\mathbf{H}_c$, called a coercive magnetic field.

Let us consider a ferromagnetic medium inside a domain $\Omega \subset \mathbb{R}^3$. We denote with $\mathbf{E}$ the electric field, $\mathbf{H}$ the magnetic field, $\mathbf{D}$ the electric displacement, $\mathbf{B}$ the magnetic induction field. In the classical theory of electromagnetism, a ferromagnetic material is described by the following constitutive equations

$$\mathbf{D}(\mathbf{x},t) = \varepsilon(\mathbf{x})\,\mathbf{E}(\mathbf{x},t)\,, \tag{3.1}$$

$$\mathbf{B}(\mathbf{x},t) = \mu(\mathbf{x})\,\mathbf{H}(\mathbf{x},t) + \mathbf{M}\left[\mathbf{H}(\mathbf{x},t)\right]. \tag{3.2}$$

here $\varepsilon(\mathbf{x})$ and $\mu(\mathbf{x})$ denote, respectively, the electric and magnetic permittivity of the material, while $\mathbf{M}$ denotes the magnetization field, which is a multi–valued function of $\mathbf{H}$. The characteristic behaviour of a magnetic material is described by a magnetization curve by plotting the intensity of the magnetic induction field $\mathbf{B}$ against the strength of the magnetic field $\mathbf{H}$. This curve is represented by a hysteresis loop (see Fig.1), typical of the behaviour of a ferromagnetic material. The proposed model describes a hard magnet. That is a metal having a high coercive force which gives a large magnetic hysteresis.

The equation (4.6), relating the variation of the magnetization $\mathbf{M}$ to the magnetic field $\mathbf{H}$ is a complex constitutive function. The choice of such a law is appropriate in order to model the phenomenon as a phase transition.

Within this approach, we suggest and scrutinize here a phase–field model that sets the phenomenon in the general framework of the Ginzburg–Landau theory of a second order phase transition [21].

The common behavior shown during the paramagnetic–ferromagnetic phase transition is due to a change of the order in the internal structure that the two phases exhibit. In this situation, the change of the order is associated to a breaking of symmetry.

In order to model all the phase transitions from a macroscopic point of view, we will suppose that the order of the structure of the material under consideration can be represented by means of a variable, called an order parameter according to Landau. The choice of the order parameter is the first step in the study of phase transitions.

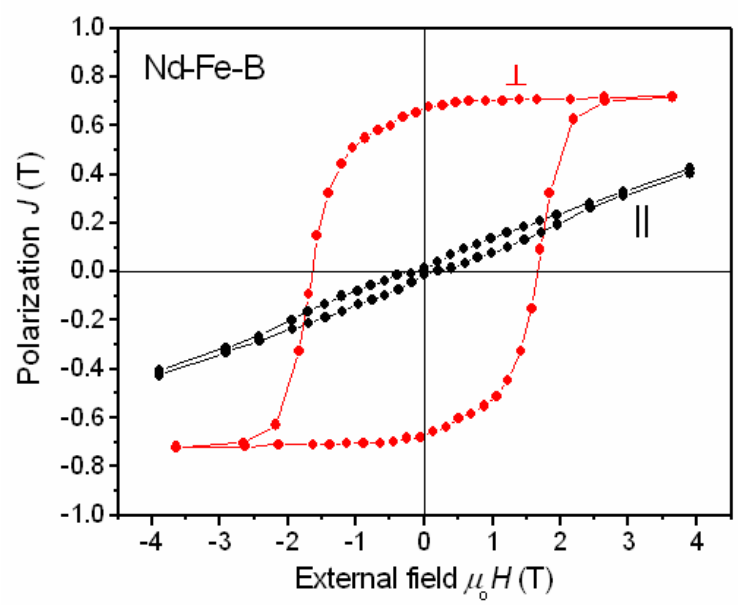

Figure 3.1: Hysteresis loop of a Nd-Fe-B film in a H-M diagram

In most applications, the order parameter is identified by a scalar variable, but it can be a vector or a tensor parameter as in some models of liquid crystals where it is the macroscopic average of the dielectric tensor.

For instance in ferromagnetism the point of view we will adopt here identifies the components of the magnetization field $\mathbf{M}$ with the set of parameters able to characterize the "amount of order" of the internal structure of the material. Since the order parameter $\mathbf{M}$ is a vector, the model takes into account not only the number of orientated spins, but also their direction. Accordingly, the magnetization $\mathbf{M}(\mathbf{x}, t)$ is identified as the phase field which is a vector–valued rather than a scalar–valued field.

According to this assumption, we deduce a model of the phenomenon, which allows a more direct comparison with other classical models of ferromagnetism, and is based on the introduction of two distinct evolution equations for the modulus $f[\varphi(\mathbf{x}, t)]$ and the direction $\mathbf{m}(\mathbf{x}, t)$ of the magnetic vector $\mathbf{M}$, by means of the following decomposition

$$\mathbf{M} = f(\varphi)\mathbf{m},$$

here the variable $\varphi(\mathbf{x}, t)$ can be interpreted as a phase field which satisfies the Ginzburg–Landau equation. The evolution equation of the vector $\mathbf{m}$ will be described by the classical Landau–Lifshitz- Gilbert equation.

In the descriptions of the phenomena related to phase transitions, we will suppose that the equations governing the evolution of the order parameter can be obtained from a balance law.

Indeed, we will assume that the variation of the structure order inside the material, is balanced by the flux of the order entering the boundary and an increase due to possible

external sources [5], [14], [28].

To this new balance equation on the order of the structure, we will associate a new form of energy which has to be considered in the formulation of the first law of thermodynamics. In other words, during a phase transition, the change of the order of structure yields a variation of internal power of the material, which will be involved in the energy balance [21].

To this purpose, let us consider the domain $\Omega \subset \mathbb{R}^3$ occupied by the material. For any subdomain $S \subset \Omega$, the new balance law is expressed by the equality

$$\int_S \rho k dx = \int_{\partial S} \mathbf{p} \cdot \mathbf{n} d\sigma + \int_S \rho \delta dx \qquad \forall S \subset \Omega.$$

where ρ is the mass density and k will be called the internal specific structure order, while $\mathbf{p}$ and δ denote respectively the flux vector and the source of the structure order.

The arbitrariness of S and the divergence theorem lead to the local equation

$$\rho k = \nabla \cdot \mathbf{p} + \rho \delta, \tag{3.3}$$

It is worth noting that the class of transitions can be divided into two parts: phase transitions with conserved order parameter and phase transitions with non–conserved order parameter. Examples of the former kind are the transition occurring in a binary alloy, where the order parameter is related to the density of one component. Clearly, the two components retain their masses unchanged even during the transition. This is the reason for the "conserved–order parameter".

Instead most of the transitions that we consider are characterized by a "non–conserved order parameter". For instance, in an ice–water transition, the order parameter, identified with the water density, is not conserved, since the whole solid component can melt into the liquid component or vice versa, according to the value of the temperature.

3.3 Ginzburg–Landau equation

In this section we will analyze only transitions with a non–conservative order parameter. In order to describe the behavior of the transition, we have to identify the set of variables able to characterize the state. In the simplest model, the state of the material coincides with the triplet $\sigma = (\varphi, \nabla\varphi, \theta)$, where φ is the order parameter and θ is the variable which controls the transition. For instance, θ is the absolute temperature, which induces the phase transition.

We consider homogeneous materials, so that the mass density ρ is constant. In the following, we let $\rho = 1$. Moreover, we assume that φ is scalar–valued and θ_c is the temperature at the transition, called the Curie temperature.

The choice of the order parameter identifies the kind of the transition. In agreement with Landau theory, it is usually assumed that

(i) φ is bounded with values in the interval $[-1, 1]$;

(ii) φ is zero in the less ordered phase and non–zero in the more ordered phase.

In particular if $\varphi = 0$ the material is in a paramagnetic phase, while if $\varphi \neq 0$ the material is in a ferromagnetic phase.

In order to characterize the phase transition, we have to specify the constitutive equations for the quantities k([1]) and $\mathbf{p}$ occurring in the balance equation (4.8), while the external source δ is required to vanish. We express k and $\mathbf{p}$ in terms of order parameter as

$$k = \tau\varphi_t + \theta_c F'(\varphi) + (\theta - \alpha\mathbf{H}\cdot\mathbf{m})\, G'(\varphi) - sign(\varphi)\,\mathbf{H}\cdot\mathbf{m}, \tag{3.4}$$

$$\mathbf{p} = \frac{1}{\kappa^2}\nabla\varphi, \tag{3.5}$$

where τ, α and κ^2 are positive constants and F', G' are derivatives of two functions depending only on φ. The choice of the functions F and G identifies different models of transition phase. As in [21], [5], for a classical second order phase transition, we suppose

$$F(\varphi) = \frac{1}{4}\varphi^4 - \frac{1}{2}\varphi^2, \qquad G(\varphi) = \frac{1}{2}\varphi^2, \tag{3.6}$$

Moreover, by (4.11) and (4.12), equation (4.8) yields the following equation that describes the evolution of the order parameter φ

$$\tau\varphi_t = \frac{1}{\kappa^2}\triangle\varphi - \theta_c F'(\varphi) - (\theta - \alpha\mathbf{H}\cdot\mathbf{m})\, G'(\varphi) + sign(\varphi)\,\mathbf{H}\cdot\mathbf{m}, \tag{3.7}$$

This is the real Ginzburg–Landau equation typical of para–ferromagnetic phase transition models.

3.4 Landau–Lifshitz equation

In 1935, Landau and Lifshitz [35] proposed a phenomenological theory developed later by Brown [15] and Prohl [46] (see also [33]) known as micromagnetics. The model describes the behaviour of a rigid ferromagnetic body in isothermal conditions below the Curie temperature. When the material is saturated, the magnetization field $\mathbf{M}$ is given by

$$\mathbf{M} = M_s\mathbf{m},$$

where M_s, constant, is the magnetic induction at saturation and $\mathbf{m}$ is a unimodular vector.

The equation governing the evolution of $\mathbf{m}$ is assumed to be

$$\mathbf{m}_t = -\gamma\mathbf{m}\times\mathbf{H}, \tag{3.8}$$

with γ a positive constant called the gyromagnetic ratio.

This equation allows us to explain a precession of $\mathbf{m}$ around the direction of the magnetic field $\mathbf{H}$. In order to include dissipative effects, a further term should be added to (4.14) which pushes the magnetization $\mathbf{M}$ towards $\mathbf{H}$. Thus equation (4.14) is modified as in [27] to

[1] It is easy observe that in the conservative case the function k, appearing in the balance equation (4.8), is proportional to the time derivative of the order parameter, namely $k = \tau\dot{\varphi}$. This is not the case in the non–conservative assumption, where k has a more involved expression.

$$\mathbf{m}_t = -\gamma \mathbf{m} \times \mathbf{H} - \lambda \mathbf{m} \times (\mathbf{m} \times \mathbf{H}),$$

where γ and λ are two positive constants.

In this framework, in order to take into account the phase change we consider a modified Landau–Lifshitz equation

$$G(\varphi)\, \mathbf{m}_t = -\gamma \mathbf{m} \times \mathbf{H} - \lambda \mathbf{m} \times (\mathbf{m} \times \mathbf{H}). \tag{3.9}$$

By this last equation, (3.9), we obtain for $G(\varphi) = 0$, the magnetization $\mathbf{M}$ and the magnetic field $\mathbf{H}$ are parallel.

The differential system is completed by Maxwell equations given by

$$\frac{\partial \mathbf{D}}{\partial t} = \nabla \times \mathbf{H} - \mathbf{J}, \qquad \nabla \cdot \mathbf{D} = \rho, \tag{3.10}$$

$$\frac{\partial \mathbf{B}}{\partial t} = -\nabla \times \mathbf{E}, \qquad \nabla \cdot \mathbf{B} = 0, \tag{3.11}$$

where ρ is the electric charge density and $\mathbf{J}$ is the electric current.

3.5 Thermodynamic restrictions

In this section, we prove the compatibility of the model with thermodynamic laws. In this situation, we choose equation (3.7), which governs the evolution of the phase field $\varphi(\mathbf{x}, t)$.

For the sake of simplicity, we assume $\kappa = 1$. Let us multiply the equation (3.7) by φ_t. This leads by the divergence theorem, we get

$$\tau \varphi_t^2 + \theta_c F_t(\varphi) + (\theta - \alpha \mathbf{m} \cdot \mathbf{H}) G_t(\varphi) - sign(\varphi)\, \varphi_t \mathbf{m} \cdot \mathbf{H} +$$

$$+ \left(\frac{1}{2} |\nabla \varphi|^2 \right)_t = \nabla \cdot (\varphi_t \nabla \varphi). \tag{3.12}$$

Further, we add to equation (4.15) a new constitutive equation which replaces equation (4.6). Namely

$$\mathbf{B}_t = \mu \mathbf{H}_t + \alpha (G(\varphi)\, \mathbf{m})_t + sign(\varphi)\, \varphi_t \mathbf{m}. \tag{3.13}$$

Now, to verify the principles of thermodynamics, we need to define the internal power associated to the equations (4.3), (3.7), (4.16).

Indeed, the "First Law of Thermodynamics" contains a state function $e(\mathbf{x}, t)$, called internal energy, such that

$$e_t = \mathcal{P}_s^{(i)} + h, \tag{3.14}$$

where $\mathcal{P}_s^{(i)}$ is the internal power of the system and h is the heat power defined by the rate at which heat is absorbed per unit mass and time. Accordingly, in the energy balance law (4.17),

we must introduce the definition of the internal power. In this model we denote with $\mathcal{P}_{el}^{(i)}$, $\mathcal{P}_{ma}^{(i)}$ and $\mathcal{P}_{\varphi}^{(i)}$ the internal electric, magnetic and chemical powers respectively. Therefore, (4.17) leads to equation

$$e_t = \mathcal{P}_{el}^{(i)} + \mathcal{P}_{ma}^{(i)} + \mathcal{P}_{\varphi}^{(i)} + h. \tag{3.15}$$

So that, from Maxwell equations, (4.1) and (4.3), we obtain the internal electric power $\mathcal{P}_{el}^{(i)}$, which, by (4.5), can be represented in the usual form, without the term $\mathbf{J} \cdot \mathbf{E}$([2]),

$$\mathcal{P}_{el}^{(i)} = \mathbf{D}_t \cdot \mathbf{E} = \varepsilon \mathbf{E}_t \cdot \mathbf{E}, \tag{3.16}$$

Moreover, from (4.16), we obtain the internal magnetic power

$$\mathcal{P}_{ma}^{(i)} = \mathbf{B}_t \cdot \mathbf{H} = \mu \mathbf{H}_t \cdot \mathbf{H} + (\alpha G_t(\varphi) + \varphi_t sign(\varphi)) \mathbf{m} \cdot \mathbf{H} + \alpha\lambda |\mathbf{m} \times \mathbf{H}|^2 \tag{3.17}$$

Finally, by (4.15) we obtain the internal structural power

$$\mathcal{P}_{\varphi}^{(i)} = \tau\varphi_t^2 \ + \theta_c F_t(\varphi) + (\theta - \alpha \mathbf{m} \cdot \mathbf{H}) G_t(\varphi) +$$

$$- sign(\varphi) \varphi_t \mathbf{m} \cdot \mathbf{H} + \left(\frac{1}{2} |\nabla\varphi|^2 \right)_t. \tag{3.18}$$

Then (4.18), by (3.16), (3.17) and (3.18), yields

$$e_t = \frac{1}{2} \left(\varepsilon |\mathbf{E}|^2 + \mu |\mathbf{H}|^2 + |\nabla\varphi|^2 \right)_t + \theta_c F_t(\varphi) + \tau\varphi_t^2 + \theta G_t(\varphi) +$$

$$+ \alpha\lambda |\mathbf{m} \times \mathbf{H}|^2 + h. \tag{3.19}$$

A complete description of para–ferromagnetic phase transition requires the introduction of an equation that defines the evolution of the temperature. Therefore, we introduce the heat balance law by the equation (see [21])

$$h = -\nabla \cdot \mathbf{q} + r, \tag{3.20}$$

where $\mathbf{q}$ denotes the heat flux vector and r the heat supply. In this frame–work, we suppose the heat flux vector is defined by the classical Fourier law

$$\mathbf{q} = -k^* \ \nabla\theta, \tag{3.21}$$

where θ is the absolute temperature and $k^* > 0$ the thermal conductivity of the material, which we consider as a constant([3]). In the following we choose $\hat{e}$ such that $\hat{e}_\theta = a_0 > 0$. Then

$$e(\theta, \varphi, \mathbf{E}, \mathbf{H}, \nabla\varphi) = a_0\theta + \frac{1}{2} \left(\varepsilon |\mathbf{E}|^2 + \mu |\mathbf{H}|^2 + |\nabla\varphi|^2 \right) + \theta_c F(\varphi),$$

[2] Its effect is of very small magnitude.

[3] Really k^* depends upon the absolute temperature θ.

Hence, by (4.19), (4.20) and (4.21), we have the heat equation

$$\theta_t \hat{e}_\theta - \tau\varphi_t^2 - \alpha\lambda \left|\mathbf{m}\times\mathbf{H}\right|^2 - \theta G_t(\varphi) = k\Delta\theta + r. \tag{3.22}$$

In the following we choose $\hat{e}$ such that $\hat{e}_\theta = a_0 > 0$.Then, from (4.19) and (3.22), we obtain the internal energy

$$e(\theta,\varphi,\mathbf{E},\mathbf{H},\nabla\varphi) = a_0\theta + \frac{1}{2}\left(\varepsilon\left|\mathbf{E}\right|^2 + \mu\left|\mathbf{H}\right|^2 + \left|\nabla\varphi\right|^2\right) + \theta_c F(\varphi),$$

We are now in a position to prove that our model is consistent with the "Second Law of Thermodynamics". Therefore, we introduce the Clausius–Duhem inequality. There exists a state function $\eta(\mathbf{x},t)$, called entropy, such that

$$\eta_t \geqslant \frac{h}{\theta} + \frac{\mathbf{q}}{\theta^2}\cdot\nabla\theta. \tag{3.23}$$

From the definition of h, with (3.22) and inequality (3.23), we have

$$\theta\eta_t \geqslant \theta_t a_0 - \tau\varphi_t^2 - \theta G_t(\varphi) - \frac{k^*}{\theta}\left|\nabla\theta\right|^2 - \alpha\lambda\left|\mathbf{m}\times\mathbf{H}\right|^2. \tag{3.24}$$

Now, we introduce the free energy, $\psi(\mathbf{x},t) = e(\mathbf{x},t) - \eta(\mathbf{x},t)\,\theta(\mathbf{x},t)$, which, by the inequality (3.24) above, gives

$$\psi_t - \frac{1}{2}\left(\varepsilon\left|\mathbf{E}\right|^2 + \mu\left|\mathbf{H}\right|^2 + \left|\nabla\varphi\right|^2\right)_t - \theta_c F_t(\varphi) - \theta G_t(\varphi) +$$

$$-\tau\varphi_t^2 - \frac{k^*}{\theta}\left|\nabla\theta\right|^2 - \alpha\lambda\left|\mathbf{m}\times\mathbf{H}\right|^2 + \eta\theta_t \leqslant 0. \tag{3.25}$$

Inequality (3.25) admits the following choice of free energy

$$\psi = \frac{1}{2}\left(\varepsilon\left|\mathbf{E}\right|^2 + \mu\left|\mathbf{H}\right|^2 + \left|\nabla\varphi\right|^2\right) + \theta_c F(\varphi) + \theta G(\varphi) + a_0\theta - a_0\theta\log\theta. \tag{3.26}$$

Accordingly the entropy is defined as

$$\eta = -\frac{\partial\psi}{\partial\theta} = a_0\log\theta - G(\varphi). \tag{3.27}$$

Substitution of (3.27) and (3.26) into (3.25), provides the following reduced inequality

$$-\frac{k^*}{\theta}\left|\nabla\theta\right|^2 - \alpha\lambda\left|\mathbf{m}\times\mathbf{H}\right|^2 - \tau\varphi_t^2 \leqslant 0$$

This holds along any process in view of assumptions $k^* > 0$, $\tau > 0$, $\lambda > 0$ and $\alpha > 0$ together with the positiveness of the absolute temperature.

Then the thermodynamical consistence of the model is proved.

3.6 Magnetic behaviour and hysteresis loop

In this section, we prove that the model defined by equations (4.1), (4.3), (4.5), (4.6), (3.7), (4.16), (3.22) is able to describe the phenomena typical of paramagnetic–ferromagnetic behaviour, such as the hysteresis loop and the phase transition of a hard homogeneous magnet.

Let us consider the constant temperature θ, such that $\theta < \theta_c$ with the magnetic permittivity of the material μ constant. Then the material is in the ferromagnetic phase. Therefore, our model should show the typical hysteresis loop. In order to obtain this diagram, we consider a unidimensional problem, for which the phase φ belong to the interval $[-1, 1]$. In such a case, we suppose also that $\mathbf{H} = H \frac{\mathbf{H}_0}{|\mathbf{H}_0|}$, where $\mathbf{H}_0$ is the constant vector corresponding to the initial direction of $\mathbf{H}$ and

$$\mathbf{m} = sign(\varphi) \frac{\mathbf{H}_0}{|\mathbf{H}_0|}$$

Moreover, we neglect spatial variations of the field φ. Under such hypothesis, our differential problem is reduced to the following scalar system

$$\begin{cases} \tau\dot{\varphi}(t) = -\theta_c F'[\varphi(t)] - (\theta - \alpha sign(\varphi) H(t)) G'[\varphi(t)] + H(t) \\ \\ \dot{B}(t) = \mu\dot{H} + \alpha sign(\varphi) \dot{G}[\varphi(t)] + \dot{\varphi}(t), \end{cases} \tag{3.28}$$

together with the initial conditions

$$\varphi(0) = \varphi_0, \qquad B(0) = B_0. \tag{3.29}$$

In order to integrate the differential system (3.28), together with the initial conditions (3.29), which well describes the hysteresis loop related to the para–ferromagnetic phase transition for a homogeneous hard magnet, we have to specify the magnetic field $H(t)$ given in the form of a sinusoidal magnetic field

$$H(t) = H_0 \sin \omega t, \tag{3.30}$$

with frequency ω and amplitude H_0.

By choice (3.6), for F, G functions, and (3.30), for magnetic field $H(t)$, the differential system (3.28), becomes

$$\begin{cases} \tau\dot{\varphi}(t) = -\theta_c \left(\varphi(t)^3 - \varphi(t)\right) - (\theta - \alpha sign(\varphi) H_0 \sin \omega t) \varphi(t) + \\ \qquad\qquad + H_0 \sin \omega t \\ \\ \dot{B}(t) = \mu H_0 \omega \cos \omega t + \alpha sign(\varphi) \varphi(t) \dot{\varphi}(t) + \dot{\varphi}(t), \end{cases} \tag{3.31}$$

together with its initial condition

$$\varphi(0) = \varphi_0, \qquad B(0) = B_0. \tag{3.32}$$

Moreover, we also study the case in which the material is in the paramagnetic phase, namely when θ crosses θ_c. So, we prove that our model, represented by differential system (3.31), coupled with (3.32), is also able to describe a para–ferromagnetic transformation with a scalar phase transition parameter $\varphi(t)$.

3.7 Numerical Results

In this section, we study numerical behaviour of the solutions of the dimensionless system (3.31).

−**First case**.

For $\theta < \theta_c$, the numerical implementation ([4]) of the differential system (3.31) is performed with initial conditions (3.32) expressed in the form

$$\varphi_0 = 0.001, \qquad |\mathbf{B}_0| = 0, \tag{3.33}$$

and with the following choice of parameters

T	$\lvert\mathbf{H}_0\rvert$	τ	θ_c	θ	μ	α
30	15	1	40	35	10^{-3}	0.1

,

with $\omega = \frac{2\pi}{T}$, which yields the graphics of the two branches of the magnetization curve, (Fig.2). The first when $|\mathbf{H}|$ goes initially from zero to $|\mathbf{H}_0| = 15$, for $0 < t < \frac{15}{2}$ and the second when $|\mathbf{H}|$ goes from zero to $-|\mathbf{H}_0| = -15$, for $\frac{15}{2} < t < \frac{45}{2}$,

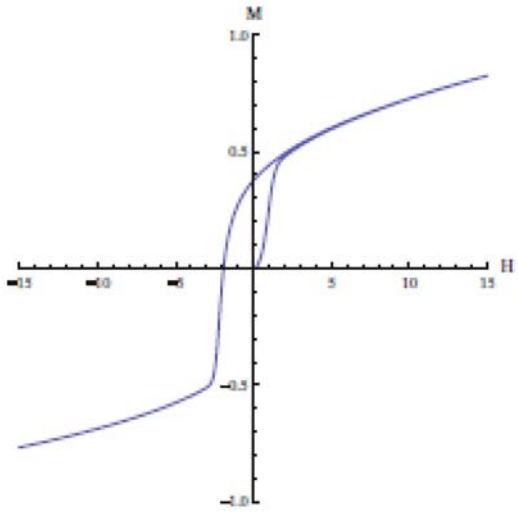

Figure 3.2: The first two branches of the magnetization curve

From the shape of the first of these two branches, called "first magnetization curve", we observe that when $|\mathbf{H}|$ increases, initially $|\mathbf{B}|$ increases more quickly and then more slowly, until, for higher values of $|\mathbf{H}|$, the magnetization process shows a tendency to achieve a limit for $|\mathbf{B}|$ value, called the magnetic induction field at the saturation $|\mathbf{B}_s| = 0.82$. If we now decrease $|\mathbf{H}|$, for $\frac{15}{2} < t < 15$, then also the magnetic induction field also decreases, but the

[4]The numerical implementation has been conducted by the differential numeric algorithms within Wolfram *Mathematica 7* code.

system state is such that the magnetic induction field $|\mathbf{B}|$ cannot recover to the original first magnetization branch exactly. In fact, for $t = 15$, $|\mathbf{B}|$ overtakes the $|\mathbf{H}| = 0$ value, and there exists a $|\mathbf{B}_r| = 0.38 \neq 0$ value, called the residual magnetic induction of the material. To reduce $|\mathbf{B}_r|$ to zero, one needs, for $15 < t < \frac{45}{2}$, to apply a magnetic field $-|\mathbf{H}_c| = -1.92$, for $t \simeq 16$, called the coercive magnetic field. If, for $16 < t < \frac{45}{2}$, we now decrease negatively the magnetic field, that is to say we increase its modulus, the material magnetizes itself in a contrary direction compared to the previous case, since the magnetic induction reaches a new saturation value $-|\mathbf{B}'_s| = -0.77 \neq 0$, for $t = \frac{45}{2}$.

If we reverse $|\mathbf{H}|$ from -15 to 15, for $\frac{45}{2} < t < \frac{75}{2}$, the magnetization curve displays a third branch (Fig.3)

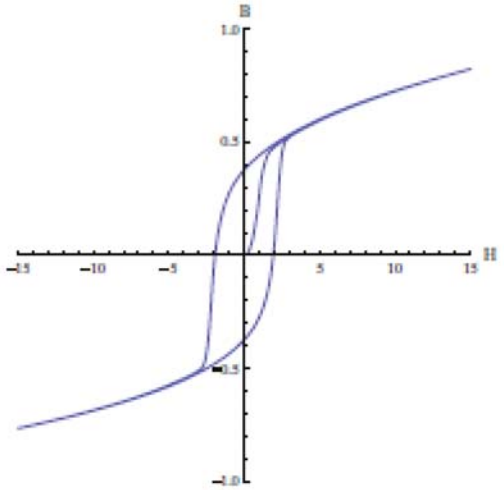

Figure 3.3: Hysteresis cycle with $\theta_1 < \theta_c$

From Fig.3, we observe that these three magnetization curves shape a loop. In particular, for $\frac{45}{2} < t < 30$, when $|\mathbf{H}|$ increases negatively to zero, that is to say when we decrease its modulus, we obtain again, for $t = 30$, a new residual magnetic induction $-|\mathbf{B}'_r| = -0.37 \neq 0$, which can be removed by a new coercive magnetic field $|\mathbf{H}'_c| = 1.93$, for $t \simeq 31$. Then, for $31 < t < \frac{75}{2}$, if we increase $|\mathbf{H}|$ it finally overtakes the saturation with a new magnetic saturation value $|\mathbf{B}''_s| = 0.82$. The phenomenon, previously described, by which the magnetic induction $|\mathbf{B}|$ differs from magnetic field $|\mathbf{H}|$, is called "magnetic hysteresis" and, by consequence, the loop represented in Fig.3, which is in good agreement with the experimental results for a ferromagnetic–paramagnetic transition phase, is called "magnetic hysteresis loop".

In the next table we report the characteristic values of the order parameter φ

$\varphi_{\lvert\mathbf{B}_s\rvert}$	$\varphi_{\lvert\mathbf{B}_r\rvert}$	$\varphi_{-\lvert\mathbf{H}_c\rvert}$	$\varphi_{-\lvert\mathbf{B}'_s\rvert}$	$\varphi_{-\lvert\mathbf{B}'_r\rvert}$	$\varphi_{\lvert\mathbf{H}'_c\rvert}$	$\varphi_{\lvert\mathbf{B}''_s\rvert}$
0.79	0.38	$3 \cdot 10^{-3}$	-0.77	-0.38	10^{-3}	0.79

.

–**Second case**.

For $\theta < \theta_c$, the differential system (3.31), solved with the same initial conditions (3.33) but with the following parameters

T	$\lvert\mathbf{H}_0\rvert$	τ	θ_c	θ	μ	α
30	15	1	40	25	10^{-4}	10^{-2}

,

yields the following magnetic hysteresis loop of a hard magnets

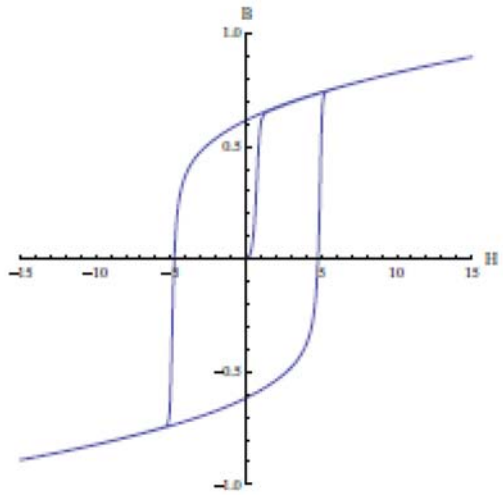

Figure 3.4: Hysteresis cycle with $\theta_2 < \theta 1 < \theta_c$

The numerical results, together with characteristic values of the order parameter φ, are

$\lvert\mathbf{B}_s\rvert$	$\lvert\mathbf{B}_r\rvert$	$-\lvert\mathbf{H}_c\rvert$	$-\lvert\mathbf{B}'_s\rvert$	$-\lvert\mathbf{B}'_r\rvert$	$\lvert\mathbf{H}_c\rvert$	$\lvert\mathbf{B}''_s\rvert$
0.896	0.616	-4.77	-0.891	-0.616	4.78	0.896

,

$\varphi_{\lvert\mathbf{B}_s\rvert}$	$\varphi_{\lvert\mathbf{B}_r\rvert}$	$\varphi_{-\lvert\mathbf{H}_c\rvert}$	$\varphi_{-\lvert\mathbf{B}'_s\rvert}$	$\varphi_{-\lvert\mathbf{B}'_r\rvert}$	$\varphi_{\lvert\mathbf{H}'_c\rvert}$	$\varphi_{\lvert\mathbf{B}''_s\rvert}$
0.893	0.616	$1.48 \cdot 10^{-3}$	-0.890	-0.616	$0.52 \cdot 10^{-3}$	0.893

.

–**Third case**.

For $\theta < \theta_c$, the differential system (3.31), is solved with the same initial conditions (3.33) and the following data parameters

T	$\lvert\mathbf{H}_0\rvert$	τ	θ_c	θ	μ	α
30	15	1	40	20	10^{-5}	10^{-3}

,

yields the following magnetic hysteresis loop typical of a hard magnet

The numerical results, together with characteristic values of the order parameter φ, are

$\lvert\mathbf{B}_s\rvert$	$\lvert\mathbf{B}_r\rvert$	$-\lvert\mathbf{H}_c\rvert$	$-\lvert\mathbf{B}'_s\rvert$	$-\lvert\mathbf{B}'_r\rvert$	$\lvert\mathbf{H}_c\rvert$	$\lvert\mathbf{B}''_s\rvert$
0.946	0.708	-6.62	-0.947	-0.709	6.63	0.946

,

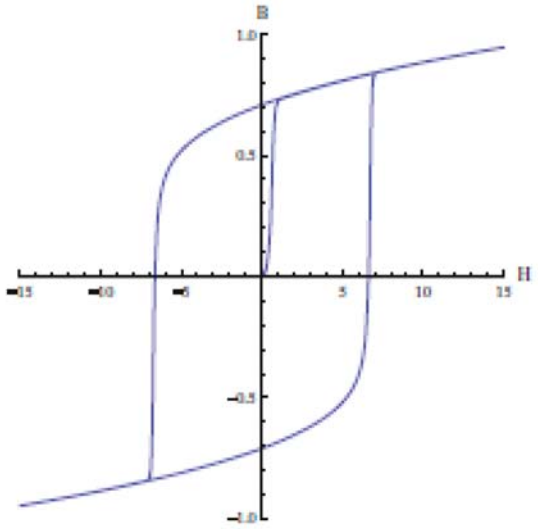

Figure 3.5: Hysteresis cycle with $\theta_3 < \theta_2$

$\varphi_{\lvert\mathbf{B}_s\rvert}$	$\varphi_{\lvert\mathbf{B}_r\rvert}$	$\varphi_{-\lvert\mathbf{H}_c\rvert}$	$\varphi_{-\lvert\mathbf{B}'_s\rvert}$	$\varphi_{-\lvert\mathbf{B}'_r\rvert}$	$\varphi_{\lvert\mathbf{H}'_c\rvert}$	$\varphi_{\lvert\mathbf{B}''_s\rvert}$
0.947	0.709	10^{-3}	-0.946	-0.709	10^{-3}	0.947

.

By observing Fig.2, Fig.3 and Fig.5, we remark that the area enclosed into hysteresis loops varies when we change the values of parameters data. In particular, we observe that generally this variation increases when the positive jump $\theta_c - \theta$ increases.

–**Fourth case**.

For $\theta > \theta_c$, the differential system (3.31), is solved with the same initial conditions (3.33), but now with the following data parameters

T	$\lvert\mathbf{H}_0\rvert$	τ	θ_c	θ	μ	α
50	15	1	20	45	10^{-4}	0.1

,

This gives the following magnetic hysteresis loop

The numerical results, together with characteristic values of the order parameter φ, are

$\lvert\mathbf{B}_s\rvert$	$-\lvert\mathbf{B}'_s\rvert$	$\lvert\mathbf{B}''_s\rvert$
0.515	-0.489	0.515

,

$\varphi_{\lvert\mathbf{B}_s\rvert}$	$\varphi_{-\lvert\mathbf{B}'_s\rvert}$	$\varphi_{\lvert\mathbf{B}''_s\rvert}$
0.509	-0.491	0.509

.

In this case, we observe that, when $\theta > \theta_c$, our model describes a para–ferromagnetic phase transition, but the magnetic behaviour of the material shows that it goes from the ferromagnetic state to the paramagnetic state.

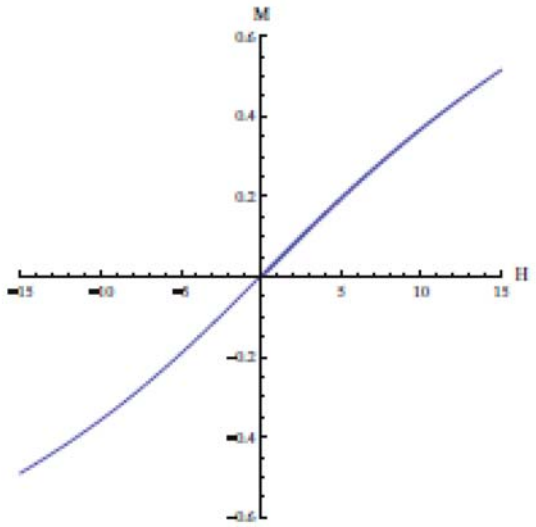

Figure 3.6: Phase diagram with $\theta_4 < \theta_c$

–**Fifth case**.

For $\theta > \theta_c$, the differential system (3.31), is solved with the same initial conditions (3.33) but now with the following data parameters

T	$\lvert\mathbf{H}_0\rvert$	τ	θ_c	θ	μ	α
50	15	1	20	80	10^{-4}	0.1

,

This now yields the following magnetic hysteresis loop of Figure 7.

The numerical results are

$\lvert\mathbf{B}_s\rvert$	$-\lvert\mathbf{B}'_s\rvert$	$\lvert\mathbf{B}''_s\rvert$
0.247	−0.246	0.247

,

together with characteristic values of the order parameter φ

$\varphi_{\lvert\mathbf{B}_s\rvert}$	$\varphi_{-\lvert\mathbf{B}'_s\rvert}$	$\varphi_{\lvert\mathbf{B}''_s\rvert}$
0.247	−0.244	0.247

.

In these last two cases, we observe that, when $\theta > \theta_c$, our model describes yet a para–ferromagnetic phase transition, but the magnetic behaviour of the material shows that it goes from the ferromagnetic state to the paramagnetic state. Besides, when the jump $\theta - \theta_c > 0$ increases, we observe that the magnetization curves become more and more linear with lower $\mathbf{B}_s$ values and with a lower $\frac{d\mathbf{B}}{d\mathbf{H}}$, in the region of thr origin.

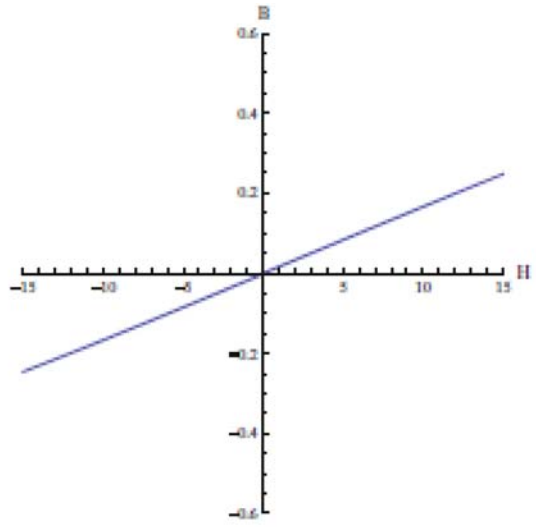

Figure 3.7: Phase diagram with $\theta_5 < \theta_4$

Chapter 4

Analysis of shape memory alloy in the phase transition approach

A model for shape memory alloys described by a intermediate pattern between a first and a second order phase transition is studied. Moreover, by the thermodynamic compatibility of the model, we provide suitable restrictions on the potentials of the Ginzburg-Landau system. Finally, we present numerical simulations of this shape memory model, which are in good agreement with experimental data [25].

4.1 Introduction

In a shape memory alloys, we observe a structural transformation between austenite and martensite phase, called martensite phase transition. These materials are capable to recover permanent strain when are heated over a given temperature. At high temperature the crystal lattice of the material is in a high symmetric phase, called austenite (A). At low temperature we observe the martensite phase (M), represented by a smaller symmetry. This transformation is crystallographically reversible (see [44]). Moreover, the variations of the stress and temperature have a large influence on these transformations. So to generate force and thermal changes through a phase transition. For the study of these materials, we follow the approach presented in the papers [7],[39], by the notion of order parameter or phase field φ and the use of the Ginzburg-Landau (G-L) theory of phase transitions, together to the classical equations of thermomechanics. In this work, compared with the works in [6], [7], we have considered two different potentials in G-L equation, which provide more convenient numerical simulations for the stress-strain diagrams. Moreover, these two new potentials are able to well describe some SMAs, as the Single Crystal AuZn (see [38],[19]), for which the character of the transformation lies at a borderline between a continuous and discontinuous phase transition. So that, this new free energy describes an intermediate behavior within a first and second order phase transition.

In other words, our differential system differs from other classic SMA models studied in [39], [40], [41], [6], [7], [23], because now the transformation is described by a continuous transition between austenite and martensite phase, as considered in [38],[19].

Following [22], [23], the G-L equation is obtained as a balance law on the internal structure of the material, and then as a new field equation to which to associate a new internal power to be considered in the First Law of Thermodynamics. In our model, the G-L, the motion and heat equations are related by a differential constitutive equation on the strain, stress and order parameter.

Finally, we study some numerical simulations for 1-D problem, for which now the order parameter and the free energy take a different representation compare to 3-D model. Nevertheless, this 1-D problem describes the same intermediate behavior between a continuous and discontinuous transitions.

Our study begin with the explicit field equations for 3-D model, describing shape memory alloys. Here, the several variants of martensite are described by the product $\varphi\varepsilon$, where ε is the strain, fixed by crystallographic structure and $\varphi \in [0, 1]$. The model is in agreement with the typical damping capacity and fatigue life of a SMAs. Then, we study the compatibility of the model with the Thermodynamic Laws. So, we obtain the potentials: internal energy, free energy and entropy. In the last section, we present a one-dimensional model, for which now the order parameter $\varphi \in [-1, 1]$. Thus, this model is not a special case of the 3-D model. The chapter finishes with some numerical simulations, that provide the classical stress-strain diagrams of SMAs.

4.2 Austenite-martensite 3-D Model

We proceed building a differential system by the Landau theory on phase transitions, using the notion of order parameter φ. For 3-D model the austenite phase will be denoted by $\varphi = 0$, while the martensite phase with $\varphi > 0$. Now we suggest for the phase field of shape memory alloys, the following Gibbs free energy, as a function of the absolute temperature θ, strain tensor ε, order parameter φ and its gradient $\nabla\varphi$

$$\begin{aligned}\rho_0\Psi(\theta,\varphi,\nabla\varphi,\varepsilon) &= \rho_0\Psi_0(\theta) + \frac{1}{2}\lambda\varepsilon\cdot\varepsilon + \frac{\kappa}{2}(\nabla\varphi)^2 + \theta_c F(\varphi) + \\ &\quad \left(\hat{\theta}_c - \alpha|\varepsilon|\right) G(\varphi) \end{aligned} \tag{4.1}$$

where ρ_0 is the reference density, λ a positive defined four order tensor, κ and α two positive constants and θ_c a fixed temperature. While, the function $\hat{\theta}_c$ is given by

$$\hat{\theta}_c = \begin{cases} \theta & \text{for} \quad \theta > \theta_c \\ \theta_c & \text{for} \quad \theta \leq \theta_c \end{cases}$$

So, from (4.1) and by the classical formula

$$\gamma\dot{\varphi} = -\frac{\delta}{\delta\varphi}\left[\rho_0\Psi(\theta,\varphi,\nabla\varphi,\varepsilon)\right] \tag{4.2}$$

we obtain the G-L equation

$$\gamma\dot{\varphi} = \kappa\nabla^2\varphi - \theta_c F'(\varphi) - (\hat{\theta}_c - \alpha|\varepsilon|)G'(\varphi). \tag{4.3}$$

where, with the dot we denote the total time derivative. Finally, the functions F and G are two potentials defined by the polynomials

$$F(\varphi) = \frac{\varphi^4}{4} - \frac{2}{3}\varphi^3 + \frac{\varphi^2}{2}, \qquad G(\varphi) = \begin{cases} 0 & if \quad \varphi \leq 0 \\ -\dfrac{\varphi^4}{4} + \dfrac{\varphi^2}{2} & if \quad 0 < \varphi < 1 \\ \dfrac{1}{4} & if \quad \varphi \geq 1 \end{cases} \tag{4.4}$$

In a stationary state, when $\theta_c > (\hat{\theta}_c - \alpha|\boldsymbol{\varepsilon}|)$, the material is in martensite phase (**M**), while for $\theta_c < (\hat{\theta}_c - \alpha|\boldsymbol{\varepsilon}|)$, we are in austenite phase (**A**). The strip enclosed inside θ_c and $\hat{\theta}_c$ represents the area in which we observe the phase transition. The classical phase diagram for a shape memory alloys is represented in the Fig.1.

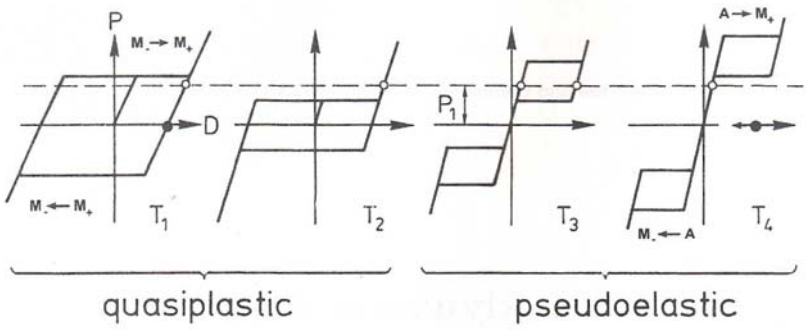

Figure 4.1: HTypical SMA cyclic stress processes for different temperatures (Mueller - Seelecke. Math.Comp.Mod. 2000).

In order to complete the differential system, we have to introduce the motion equation

$$\rho_0 \ddot{\mathbf{u}} = \nabla \cdot \boldsymbol{\sigma} + \rho_0 \mathbf{b} \tag{4.5}$$

where $\mathbf{u}$ is the displacement and $\mathbf{b}$ the body force.

The behavior of a SMA is described by the constitutive equation among σ, ε and φ. For this 3-D model, we put

$$\dot{\varepsilon} = \lambda^{-1}\dot{\sigma} + \varkappa \left(\frac{\varepsilon}{|\varepsilon|}\right)^{\cdot} G(\varphi) \tag{4.6}$$

where the tensor $\varkappa = \alpha\lambda^{-1}$.

4.3 Energy balance and Second Law of Thermodynamics

For achieving to First Law of Thermodynamics, we need to define the internal mechanical and structural power which we denote respectively with $\mathcal{P}^i_m$, $\mathcal{P}^i_s$, besides the internal heat power $\mathcal{P}^i_\theta$.

By the equation (4.3), (4.5) and (4.6) we have

$$\mathcal{P}^i_m = \sigma \cdot \dot{\varepsilon} = \lambda\varepsilon \cdot \dot{\varepsilon} - \alpha\,|\varepsilon|^{\cdot}\, G(\varphi) \tag{4.7}$$

$$\mathcal{P}^i_s = \gamma\dot{\varphi}^2 + \left[\frac{\kappa}{2}(\nabla\varphi)^2\right]^{\cdot} + \theta_c \dot{F}(\varphi) + \left(\hat{\theta}_c - \alpha\,|\boldsymbol{\varepsilon}|\right)\dot{G}(\varphi) \tag{4.8}$$

Moreover, from the First Law of Thermodynamics we obtain the equation

$$\rho_0 \dot{e} = \mathcal{P}^i_m + \mathcal{P}^i_s + \mathcal{P}^i_\theta . =$$

$$= \lambda\varepsilon \cdot \dot{\varepsilon} + \gamma\dot{\varphi}^2 + \left[\frac{\kappa}{2}(\nabla\varphi)^2\right]^{\cdot} - (\alpha\,|\boldsymbol{\varepsilon}|\,G(\varphi))^{\cdot} + \theta_c \dot{F}(\varphi) + \hat{\theta}_c \dot{G}(\varphi) + \mathcal{P}^i_\theta \, . \tag{4.9}$$

In the following, we use the new function

$$\tilde{\theta}_c = \begin{cases} \theta - \theta_c & \text{for} \quad \theta > \theta_c \\ 0 & \text{for} \quad \theta \leq \theta_c \end{cases}$$

so that,

$$\hat{\theta}_c \dot{G}(\varphi) = \theta_c \dot{G}(\varphi) + \tilde{\theta}_c \dot{G}(\varphi)$$

Then, the equation (4.9) can be written in the new form

$$\begin{aligned} \rho_0 \dot{e} &= \frac{d}{dt}\left(\frac{1}{2}\lambda \boldsymbol{\varepsilon} \cdot \boldsymbol{\varepsilon} + \frac{\kappa}{2}(\nabla\varphi)^2 + (\theta_c - \alpha|\boldsymbol{\varepsilon}|)G(\varphi) + \theta_c F(\varphi)\right) \\ &+\gamma\dot{\varphi}^2 + \tilde{\theta}_c \dot{G}(\varphi) + \mathcal{P}_\theta^i \end{aligned} \tag{4.10}$$

Finally, we introduce the heat balance law

$$\mathcal{P}_\theta^i = -\nabla \cdot \mathbf{q} + \rho_0 r \tag{4.11}$$

where $\mathbf{q}$ is the heat flux and r is the heat supply. Finally by (4.9) and (4.11) we have the heat equation

$$\rho_0 e_\theta \dot{\theta} - \gamma\dot{\varphi}^2 - \tilde{\theta}_c \dot{G}(\varphi) = -\nabla \cdot \mathbf{q} + \rho_0 r \tag{4.12}$$

Moreover from (4.9) we obtain the internal energy

$$\begin{aligned} e(\theta,\ \varphi,\ \nabla\varphi, \boldsymbol{\varepsilon}) &= e_1(\theta) + \frac{1}{2}\lambda \boldsymbol{\varepsilon} \cdot \boldsymbol{\varepsilon} + \\ &\frac{\kappa}{2}(\nabla\varphi)^2 + (\theta_c - \alpha|\boldsymbol{\varepsilon}|)G(\varphi) + \theta_c F(\varphi) \end{aligned} \tag{4.13}$$

Therefore, the differential system is given by the equations (4.1), (4.2), (4.3) and (4.8). Now, we study the compatibility of this system with the Second law of Thermodynamics represent by means of the inequality

$$\rho_0 \dot{\eta} \geq \frac{\mathcal{P}_\theta^i}{\theta} + \frac{1}{\theta^2}\mathbf{q} \cdot \nabla\theta \tag{4.14}$$

where η is the entropy. Then, because by (4.11) and (4.12) we have

$$\mathcal{P}_\theta^i = \rho_0 e_\theta \dot{\theta} - \gamma\dot{\varphi}^2 - \tilde{\theta}_c \dot{G}(\varphi) \tag{4.15}$$

So that, the inequality (4.14) assumes the form

$$\rho_0 \dot{\eta}\theta \geq \rho_0 e_\theta \dot{\theta} - \gamma\dot{\varphi}^2 - \tilde{\theta}_c \dot{G}(\varphi) + \frac{1}{\theta}\mathbf{q} \cdot \nabla\theta. \tag{4.16}$$

There, under the hypothesis for the entropy

$$\eta(\theta,\varphi) = \eta_0(\theta) + \eta_1(\varphi,\theta)$$

and from (4.16) we have

$$\eta_1(\varphi,\theta) = \begin{cases} G(\varphi) & \text{for} \quad \theta > \theta_c \\ 0 & \text{for} \quad \theta \leq \theta_c \end{cases} \tag{4.17}$$

while $\eta_0(\theta)$ is such that

$$\theta\eta_{0\theta}\dot{\theta} - e_{1\theta}\dot{\theta} = 0 \ .$$

So

$$\eta_0 = \int \frac{e_{1\theta}}{\theta} d\theta.$$

Hence, the inequality (4.14) is satisfied if

$$\gamma\dot{\varphi}^2 + \frac{1}{\theta}\mathbf{q}\cdot\nabla\theta \geq 0 \ . \tag{4.18}$$

Finally, the free energy $\Psi = e - \theta\eta$ is given by

$$\begin{aligned} \rho_0\Psi &= \rho_0\left(e_1 - \theta\int\frac{e_{1\theta}}{\theta}d\theta\right) + \frac{1}{2}\lambda\varepsilon\cdot\varepsilon - \alpha|\boldsymbol{\varepsilon}|G(\varphi) \\ &\quad + \frac{\kappa}{2}(\nabla\varphi)^2 + \theta_c F(\varphi) - \tilde{\theta}_c G(\varphi) \end{aligned} \tag{4.19}$$

So that, from (4.19) we obtain again the equation (4.3) by the classical formula (4.2). Moreover, we have that

$$\Psi_0 = \left(e_1 - \theta\int\frac{e_{1\theta}}{\theta}d\theta\right)$$

4.4 Austenite-martensite 1-D Model

For 1-D problem, we suppose the displacement $\mathbf{u} = u(x,t)\mathbf{k}$, where $\mathbf{k}$ is a unit vector. So, we put $\varepsilon = \dfrac{\partial u}{\partial x}$, while

$$\boldsymbol{\sigma} = \begin{bmatrix} \sigma_{11} & 0 & 0 \\ 0 & 0 & 0 \\ 0 & 0 & 0 \end{bmatrix}$$

in the following the component σ_{11} will be denoted by σ. So that, the motion equation is given by

$$\rho_0\frac{\partial}{\partial t}u = \frac{\partial\sigma}{\partial x} + \rho_0 b$$

where ρ_0 denotes the density and b the body force.

For this 1-D model, the phase field equation (4.3) assumes the form

$$\gamma\dot{\varphi} = \kappa\nabla^2\varphi - \theta_c\tilde{F}'(\varphi) - (\hat{\theta}_c - \alpha\sigma\ sign(\varphi))\tilde{G}'(\varphi) \tag{4.20}$$

where now the potentials $\tilde{F}(\varphi)$ and $\tilde{G}(\varphi)$ are defined by the functions

$$\tilde{F}(\varphi) = \frac{\varphi^6}{6} - \frac{\varphi^4}{4}\,, \qquad \tilde{G}(\varphi) = \begin{cases} \dfrac{1}{6} & if \quad \varphi \geq 1 \\ \dfrac{\varphi^6}{6} - \dfrac{\varphi^4}{2} + \dfrac{\varphi^2}{2} & if \quad 0 < \varphi < 1 \\ \dfrac{1}{6} & if \quad \varphi \leq -1 \end{cases}$$

and where $\sigma = \sigma_0 sen\,(\omega t)$ is the cyclic stress law that acting on the sample.

Finally, for this 1-D problem, the constitutive equation analogous to (4.6) is now defined by

$$\varepsilon = \lambda^{-1}\sigma + \alpha\ sign(\varphi)\tilde{G}\,(\varphi) \tag{4.21}$$

The Gibbs free energy is now represented by the following functional

$$\rho_0\Psi = \rho_0 \begin{pmatrix} e_1 - \theta \\ \int \frac{e_{1\theta}}{\theta} d\theta \end{pmatrix} + \frac{1}{2}\lambda^{-1}\sigma^2 + \frac{\kappa}{2}\left(\nabla\varphi\right)^2 + \theta_c\tilde{F}(\varphi) - \tilde{\theta}_c\tilde{G}\,(\varphi)$$

Numerical simulations

In this section, we study numerical behavior of the solutions of the dimensioness phase field differential equation (4.20) coupled with the equation (4.21).

First case

For $\theta < \theta_c$, the numerical implementation ([1]) of the phase field differential equation (4.20) is performed by the following initial condition, at $t_0 = 0$,

$$\varphi\,(0) = 0$$

for the value of phase transition parameter and with the following choise of the other parameters

T	σ_0	γ	θ	θ_c	$\widehat{\theta}_c$	κ	α	λ
1.2	10	0.1	10^{-5}	10	10	0.3	50	1

where, for the cyclic stress law we consider $\sigma = \sigma_0 sen\,(\omega t)$, while ω is equal to $\dfrac{2\pi}{T}$. The problem carries out through two steps. The first step is that to solve the differential equation (4.20) to obtain so the $\varphi(t)$ function, the second step is that to introduce it in the eqution (4.21). In this way we are able to draw the following (σ, ε) diagrams for the SMAs submitted to the given cyclic stress law during the time interval $\left[0, \dfrac{5}{4}T\right] = [0, 1.5]$,

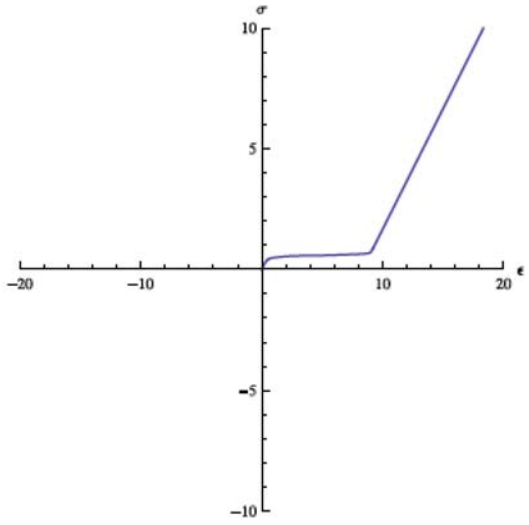

Figure 4.2: First branches for $\theta < \theta_c$and $0 < t < 0.3$.

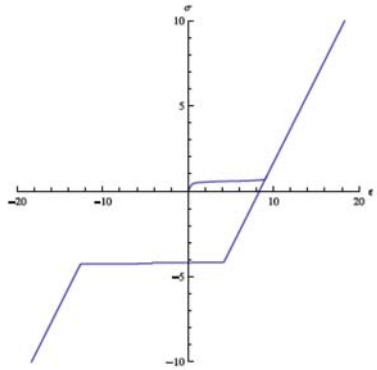

Figure 4.3: First, second and third branches for $\theta < \theta_c$ and $0 < t < 0.9$.

If we observe previous Fig.1, where the test temperature θ is smoller than the critical value θ_c, a SMAs in these condition presents a similarity with a material without a shape memory. The diagram reproduces a classic hysteresis loop model in agreement with the typical damping capacity and fatigue life of a SMAs, subject to a stress cycle inside the austenitic, in agreement with the quasi-plastic behavior of a SMAs represented to the left hand of Fig.1

Second case

For $\theta > \theta_c$, the numerical implementation of the differential equation (4.20) by the same initial condition, at $t_0 = 0$,

[1]The numerical implementation has been conducted by the differential numeric algorithms within Wolfram *Matehematica* 7 code.

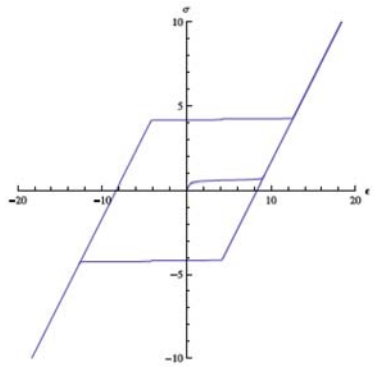

Figure 4.4: First, second, third and forth branches for $\theta < \theta_c$ and for $0 < t < 1.5$.

$$\varphi(0) = 0$$

for the value of the following phase transition parameters

T	σ_0	γ	θ	θ_c	$\widehat{\theta}_c$	κ	α	λ
1.2	6	1	150	10	150	4	40	1

where, in the cyclic stress law is alway given by $\sigma = \sigma_0 sen(\omega t)$, and ω is equal to $\dfrac{2\pi}{T}$. In this case we obbtain the following other graphics resultes.

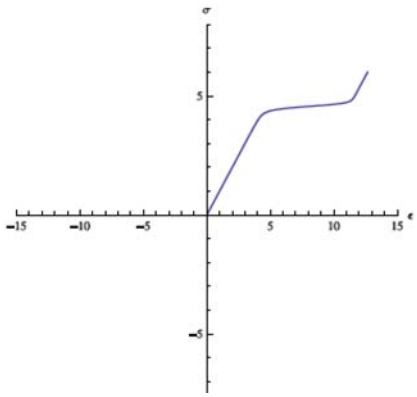

Figure 4.5: First branche for $\theta > \theta_c$and $0 < t < 0.3$.

In this second test, where the remperature is greater than the critical value θ_c, thediagrams in Fig.5, 6 and 7 show the specific beaviour of a material with shape memory. Specially, the Fig.7 reproduces a classic loop model submitted to a loading and unloading stress cycle in agreement with the pseudoelastic behavior of a SMAs, represented to the right hand of Fig.1.

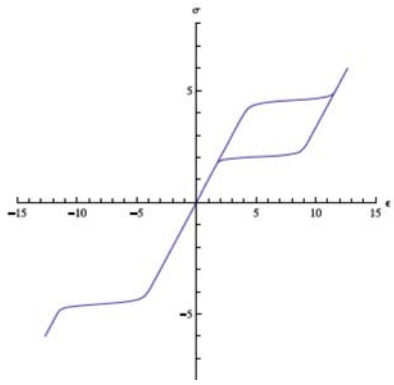

Figure 4.6: First, second and third branches for$\theta > \theta_c$ and $0 < t < 0.9$.

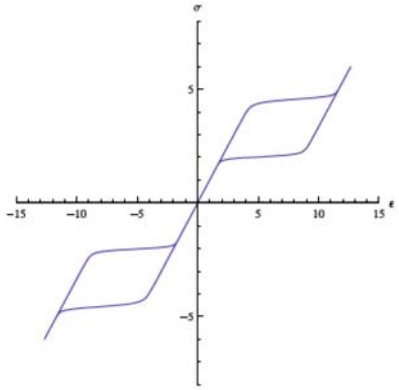

Figure 4.7: First, second and third branches for $\theta > \theta_c$ and $0 < t < 1.2$.

Bibliography

[1] Aharoni, A.: Introduction to the Theory of Ferromagnetism. Oxford University Press, Oxford (2001).

[2] A. Ascenzi, *The osteonic lamellae as elastic bodies occupying a multiply-connected region of space and their problematic*, International Congress in memory of Vito Volterra, Roma, 8-11 October 1990, printed in Atti dei Convegni Lincei, n. 92, 1992.

[3] D.M.Barnett, *Modern Dislocation theory: Extensions of the ideas of Vito Volterra*, International Congress in memory of Vito Volterra, Roma, 8-11 October 1990, printed in Atti dei Convegni Lincei, n. 92, 1992.

[4] Berti, V., Fabrizio, M.: Existence and uniqueness for a non-isothermal dynamical Ginzburg-Landau model of superconductivity. Math. Comput. Modelling. **45**, 1081-1095 (2007)

[5] Berti, V., Fabrizio, M., Giorgi, C.: A three-dimensional model in ferromagnetism. J. Math. Anal. Appl. **355,** 661–674 (2009)

[6] V. Berti, M. Fabrizio, D. Grandi, Phase transitions in shape memory alloys: a non-isothermal Ginzburg-Landau model, Physica D 239, 2010, 95-102, doi:10.1016/j.physd.2009.10.005.

[7] V. Berti, M. Fabrizio, D. Grandi, Hysteresis and phase transitions for one-dimensional and three-dimensional models in shape memory alloys, Journal of Mathematical Physics 51, 2010, 062901.

[8] K. Bhattacharya, Microstructure of Martensite, Oxford University Press, Oxford, 2003.

[9] I. Bochicchio, E. Laserra and M. Pecoraro, Sulla sesta distorsione elementare di Volterra per un cilindro cavo omogeneo e isotropo di altezza finita con carico alla Saint Venant, *Atti dell' Accademia Peloritana dei Pericolanti, Classe di Scienze Fisiche, Matematiche e Naturali*, **86** (2008).

[10] I. Bochicchio, E. Laserra and M. Pecoraro, Sul Carico alla De Saint Venant della Sesta Distorsione Elementare di Volterra, in *Math. Phys. Mod. Eng. Sciences, Societá nazionale di scienze letterarie e arti in Napoli, Studi in onore di Pasquale Renno*, Liguori Editore, pp. 9–15 (2008).

[11] I. Bochicchio, E. Laserra, M.Pecoraro, *Volterra's sixth elementary distortion: a new approach by Saint Venant's theory*, International Journal of Engineering and Interdisciplinary Mathematics, Vol. 1, N. 10, 2009.

[12] L.C. Brinson, One-dimensional constitutive behavior of shape memory alloys: thermomechanical derivation with non-constant material functions and redefined martensite internal variable, Journal of Intelligent Material Systems and Structures, 4 (1993) 229-242.

[13] M. Brocca, L.C. Brinson, Z.P. Bazant, Three-dimensional constitutive shape memory alloys based on microplane model, J. Mech. Phys. Solids 50 (2002) 1051-1077.

[14] M. Brokate, M., Sprekels, J.: Hysteresis and phase transitions. Springer, New York, (1996).

[15] Brown, W. F.: Micromagnetics. Wiley, New York, (1963).

[16] G. Caricato, *On the Volterra's distortions theory*, AIMETA '99, 14th Italian Conference on Theoretical and Applied Mechanics, Villa Olmo (Como), Italy.

[17] G. Caricato, *On the Volterra's distortions theory*, Meccanica, **35**, pp. 411–420, 2000.

[18] C. Cattani and J. Rushchitsky, Volterra's distortions in nonlinear hyperelastic media, *Int. J. of Appl. Math. and Mech.*, **3**, pp. 14–34 (2005).

[19] T.W. Darling, F. Chu, A. Migliori, D. Thoma, M. Lopez, J.C. Lashley, B.E. Lang, J. Boerio-Goates, and B.F. Woodfield, "Elastic and Thermodynamic Properties of the Shape Memory Alloy AuZn", Philos. Mag. B 82, 825-837 (2002).

[20] Fabrizio, M., Morro, A.: Electromagnetism of Continuous Media. Oxford University Press, Oxford (2003).

[21] Fabrizio M., Ginzburg-Landau equations and first and second order phase transitions. *Int. J Eng. Sci.*, **44**:529 (2006).

[22] M. Fabrizio, Ice–water and liquid–vapor phase transitions by a Ginzburg–Landau model. J. Math. Phys, 49 (2008), n.10, 102902, 13 pp.

[23] M. Fabrizio, C. Giorgi, A. Morro, A continuum theory for first-order phase transitions based on the balance of structure order, Math. Meth. Appl. Sci. 31 (2008), 627–653.

[24] M. Fabrizio, G. Matarazzo, M. Pecoraro, *Hysteresis loops for para-ferromagnetic phase transitions* , ZAMP, Springer, doi: 10.1007/s00033-011-0160, pag. 1, 2011.

[25] M. Fabrizio, M. Pecoraro, *Phase transitions and thermodynamics for the shape memory alloy AuZn*, Meccanica, vol. 48, n7, pp. 1695–1007 (2013).

[26] Fried F, Gurtin M., Continuum theory of thermally induced phase transitions based on an order parameter, *Physica D*, **68**:326 (1993).

[27] Gilbert, T.L.: A phenomenological theory of damping in ferromagnetic materials. IEEE Trans. Magnetics. **40**, 3443-3449 (2004)

[28] Goldenfeld, N.: Lectures on phase transitions and the normalization group. Addison-Wesley, Reading, Mass. (1992).

[29] R.C. Goo, C. Lexcellent, Micromechanics-based modeling of two way memory effect of a single crystalline shape memory alloy, Acta Mater. 45 (1997) 727-737.

[30] G. Grioli, *Le distorsioni elastiche e l'opera di Vito Volterra*, International Congress in memory of Vito Volterra, Roma, 8-11 October 1990, printed in Atti dei Convegni Lincei, n. 92, 1992.

[31] D. Iesan, *Saint-Venant's Problem*, Springer, 2008.

[32] Kittel, C.: Theory of the Structure of Ferromagnetic Domains in Films and Small Particles. Phys. Rev. **70**, 965-971 (1946)

[33] Kruzík, M., Prohl, A.: Recent Developments in Modeling, Analysis and Numerics of Ferromagnetism. SIAM Review. **48**, 439-483 (2006)

[34] D.C. Lagoudas, P.B. Entchev, P. Popov, E. Patoor, L.C. Brinson and X. Gao, Shape memory alloys, Part II: Modeling of polycrystals, Mechanics of Materials 38 (2006) 430-462.

x

[35] Landau, L.D., Lifshitz, E.M.: Theory of the dispersion of magnetic permeability in ferromagnetic bodies. Phys. Z. Sowietunion. **8**, 153-169 (1935)

[36] Landau, L.D., Lifshitz, E.M., Pitaevskii, L.P.: Electrodynamics of continuous media. Pergamon Press, Oxford (1984)

[37] E. Laserra and M. Pecoraro, Volterra's Theory of Elastic Dislocations For A Transversally Isotropic Homogeneous Hollow Cylinder, *Nonlinear Oscillations*, **6**, pp. 56–73 (2003).

[38] J.C. Lashley, B.E. Lang, J. Boerio-Goates, B.F. Woodfield, T.W. Darling, F. Chu, A. Migliori, and D. Thoma, "The Heat Capacity of Single Crystal AuZn Near the Martensitic Transition", J. Chem. Thermodyn. 34, 251-261 (2002).

[39] Levitas VI, Preston DL and Lee DW., Three-dimensional Landau theory for multivariant stress-induced martensitic phase transformations. I. Austenite↔martensite, *Physical review B*, **66**:134206 (2002).

[40] Levitas VI, Preston DL and Lee DW., Three-dimensional Landau theory for multivariant stress-induced martensitic phase transformations. II. Multivariant phase transformations and stress space analysis, *Physical review B*, **66**:134207 (2002).

[41] Levitas VI, Preston DL and Lee DW., Three-dimensional Landau theory for multivariant stress-induced martensitic phase transformations. III. Alternative potentials, critical nuclei, kink solutions, and dislocation theory, *Physical review B*, **68**:134201 (2003).

[42] A. E. H. Love, *The Mathematical theory of elasticity*, Cambridge University Press, Fourth edition, 1952.

[43] A.I. Lurie, *Theory of elasticity*, translated by A. Belyae, Springer, Berlin, 2005.

[44] Nishiyama Z., Martensitic Transformations. New York: Academic Press, 1978.

[45] Podio-Guidugli, P.: On dissipation mechanisms in micromagnetics. The European Physical Journal B, **19**, 417-429 (2001)

[46] Prohl, A.: Computational micromagnetism. Teubner (2001).

[47] A. Signorini, *Lezioni di Fisica Matematica*, Libreria Eredi Virgilio Veschi, Roma, 1953.

[48] K. R. Symon, *Mechanics*, Addison–Wesley, 1979.

[49] P. Villaggio, *Mathematical Models for Elastic Structures*, Cambridge University Press, Cambridge, 1998.

[50] Visintin, A.: A Weiss-type model of ferromagnetism, Physica B, **275**, 87-91 (2000)

[51] V. Volterra, Sulle distorsioni dei corpi elastici simmetrici, *Rend. Accad. Lincei*, **14** (1905).

[52] V. Volterra, *Sur l'equilibre des corps elastiques multiplement connexes*, Annales Scientifiques de l'Ecole Normale Superieure, vol. 24, pp. 401–518 (1907)

[53] C.C.Wang–C.Truesdell, *Introduction to Rational Elasticity*, Noordhoff International Publishing, 1973.

[54] M. Weingarten *Sur les surfaces de discontinuitè dans la théorie des corps solides*, Rend. Acc. Lincei, **X**, 1901, pp. 57–60.

[55] Weiss, P.: L'Hypothese du champ Moleculaire et de la Propriete Ferromagnetique. J. de Phys. **6**, (1907)

[56] L. M. Zubov, *Nonlinear Theory of Dislocations and Disclinations in Elastic Bodies* Lecture Notes in Physics Monograph, Springer, 2001.